2m11.3287.1

Université de Montréal

Dynamical properties of donor-bound excitons in Cadmium Telluride

par

Wei Li

Département de physique

Faculté des arts et des sciences

Faculté des études supérieures
Grade conféré à compter du
2005 MAI 31
Université de Montréal

Mémoire présenté à la Faculté des études supérieures

en vue de l'obtention du grade de Maîtrise ès science (M.Sc)

en Physique

March, 2005

Faculté des Études Supérieures
Grade octroyé à compter du
02 JUIN 2005
Université de Montréal

© Wei Li, 2005.

QC
3
U54
2005
v.017

Université de Montréal

Direction des bibliothèques

AVIS

L'auteur a autorisé l'Université de Montréal à reproduire et diffuser, en totalité ou en partie, par quelque moyen que ce soit et sur quelque support que ce soit, et exclusivement à des fins non lucratives d'enseignement et de recherche, des copies de ce mémoire ou de cette thèse.

L'auteur et les coauteurs le cas échéant conservent la propriété du droit d'auteur et des droits moraux qui protègent ce document. Ni la thèse ou le mémoire, ni des extraits substantiels de ce document, ne doivent être imprimés ou autrement reproduits sans l'autorisation de l'auteur.

Afin de se conformer à la Loi canadienne sur la protection des renseignements personnels, quelques formulaires secondaires, coordonnées ou signatures intégrées au texte ont pu être enlevés de ce document. Bien que cela ait pu affecter la pagination, il n'y a aucun contenu manquant.

NOTICE

The author of this thesis or dissertation has granted a nonexclusive license allowing Université de Montréal to reproduce and publish the document, in part or in whole, and in any format, solely for noncommercial educational and research purposes.

The author and co-authors if applicable retain copyright ownership and moral rights in this document. Neither the whole thesis or dissertation, nor substantial extracts from it, may be printed or otherwise reproduced without the author's permission.

In compliance with the Canadian Privacy Act some supporting forms, contact information or signatures may have been removed from the document. While this may affect the document page count, it does not represent any loss of content from the document.

Université de Montréal
Faculté des études supérieures

Ce mémoire intitulé :

Dynamical properties of donor-bound excitons in Cadmium Telluride

Présenté par :
Wei Li

À été évalué par un jury composé des personnes suivantes :

Richard Leonelli,	Directeur de recherche
Normand Mousseau,	Président-rapporteur
Carlos Silva,	Membre du jury

Mémoire accepté le : 02/05/05

To my parents for forever support from far away

To my husband for love and support

ACKNOWLEDGMENTS

I would like to express my heartfelt thanks and profound gratitude to my supervisor Prof. Richard Leonelli, not only for giving me the opportunity to work with his group but for introducing me to a new research field. I deeply appreciate that he gave me plenty of his time and educated me on various aspects of lab and experimental operations. With his kind guidance, support and encouragement, I was able to complete and well understand this work.

I also especially thank Ms. Zakia Yaïche, Mr. Collin-nadeau Brosseau, Mr. Ghaouti Bentoumi and Mr. Ali Lanacer, who gave a great help to me.

My special thanks are due to Prof. L. A. Hamel who offered us experimental samples.

I would like to thank all the members of GCM of physics department at University of Montreal.

On a personal note, I would like to thank my husband Po Dong for his support and encouragement.

I would like to thank many others who I cannot mention here by name.

SOMMAIRE

Nous étudions les propriétés dynamiques des excitons liés à des donneurs dans du tellurure de cadmium de grande pureté légèrement dopé avec des donneurs pour compenser les accepteurs. En premier lieu, nous avons réalisé une étude des profils d'émission des excitons liés au donneurs dans le CdTe. L'émission du niveau n=1 de l'exciton lié est bien reproduit par un profil de Fano, tandis que l'émission des niveau n=2, 3 correspond à un profil de Lorentz. Par la suite, nous avons effectué des mesures de photoluminescence en fonction de la température dans la plage spectrale excitonique du CdTe. Ces mesures révèlent la présence de deux mécanismes de transfert d'énergie pour les donneurs peu profonds. Jusqu'à une température d'environ 15 K, le transfert des polaritons excitoniques de la branche inférieure transverse vers la branche excitonique longitudinale domine l'évolution de la population des excitons liés. À plus haute température, la libération directe des électrons et des trous contrôle les processus de transfert.

Mots clés :

Photoluminescence, tellurure de cadmium (CdTe), profil de Fano, excitons liés, polariton

ABSTRACT

We study the dynamical properties of donor-bound excitons in high-purity cadmium telluride with low donor doping to compensate acceptors. Firstly, we performed a study of the emission lineshapes of donor-bound excitons of CdTe as a function of temperature. The emission from the n=1 donor-bound exciton matches pure and simple Fano lineshape, and the emission from n=2, 3 donor-bound excitons are well approximated by Lorentzian lineshapes. In addition, temperature-dependent photoluminescence measurements carried in the excitonic region of CdTe revealed the dynamical behavior of two energy-transfer paths for shallow donor-bound excitons. When increasing the temperature to about 15K, the energy-transfer channel from the lower-polariton-branch excitons to longitudinal excitons results in a descrease of the population of excitons bound to donors. This indicates that the drop of the integrated photoluminescence intensities is due to this exciton-transfer channel. When the temperature is further increased to 24.0 K, the liberation of free electrons and holes from donors controls the transfer process.

Key words:

Photoluminescence, cadmium telluride (CdTe), Fano lineshape, bound exciton, polariton

CONTENTS

LIST OF TABLE

LIST OF FIGURES

LIST OF SYMBOLS

β Polarizability of exciton

c Speed of light in vaccum

C_i ith constant linked to the degeneracy of $E_{t,i}$

E Reduced energy

E_f Transition energy

E_A, E_D Ionization energies of donor and acceptor impurities

E^b, E_{BX} Binding energy of free exciton to the attractive center

E_g Energy gap

E_L Longitudinal exciton energy

E_T Transverse exciton energy

$E_{T(k)}$ Transverse exciton energy at wave vector k

E_{LT}, Δ_{LT} Longitudinal-transverse exciton splitting energy

$E_{t,i}$, E_{Th} ith activation energy and thermal activation energy

E_X Binding energy of free exciton

E_0 Energy position

$E_{(D^0,X)}$, $E_{(D^+,X)}$, $E_{(A^0,X)}$ Spectral positions of (D^0,X), (D^+,X) and (A^0,X)

ε, ε_b, ε_∞ Reduced energy, low and high dielectric constant

$I^*_{(D^0,X)_{n=1,2,3}}$ Integrated PL intensities of transitions $(D^0,X)_n$

$I(E)$ Intensity at the energy E

I_i Intensity of the ith peak

$I^*(0)$ Integrated PL intensity near 0 K

kT Thermal energy at absolute temperature T

k Wave vector

m_0, m^*, m^*_{hh} Static mass of electron, electron mass and heavy-hole mass

q Fano lineshape parameter

σ Width of the spectral feature

R_0 Rydberg for the hydrogen atom

Γ Width of the spectral feature (FWHM)

(A^0,X) Neutral-acceptor-bound exciton

(A^-,X) Ionized-acceptor-bound exciton

(D^0,X) Neutral-donor-bound exciton

(D^+,X) Iionized-donor-bound exciton

$(D^0,X)_{n=1,2,3}$ n=1-3 components of the neutral-donor-bound exciton transitions $(D^0,X)_n$

X_{LPB}, X_L exciton of lower polariton branch and longitudinal exciton

CHAPTER 1

INTRODUCTION

1.1 Research motivation

In recent years, much study interest has focused on compound semiconductors InP, GaAs and CdTe. They have been widely used for the fabrication of optoelectronic devices such as GaAs/AlGaAs quantum well infrared photodetectors (QWIPs), InGaAs photodetector, CdS/CdTe solar cell, CdTe/CdZnTe based γ -Ray detectors, HgCdTe infrared detector with a CdTe buffer layer and so on, due to their excellent electronic and optical properties [1-4].

The binary compound CdTe is an important direct-band-gap II-VI semiconductor material. The band gap of CdTe is approximately 1.60 eV at low temperature, higher than those of InP and GaAs (see Table I about equivalent physical parameters of InP, GaAs and CdTe). In the past, the studies of II-VI semiconductor materials was mainly concentrated on compounds with higher band gaps such as ZnSe, ZnTe, ZnS, and CdS, but these semiconductor materials still have some fundamental difficulties in applications, since so far they cannot be well produced in both n-type and p-type forms with low resistivity [5]. However, CdTe is the only in II-VI compound semiconductors that can be

prepared in n-type, p-type, or with low resistivity [6-7]. The increasing interest in the study of CdTe is mainly in its demonstrated applications including [8]:

-solar cells (see the typical CdS/CdTe cells structure shown in Figure 1),

-γ-ray detector (CdTe/CdZnTe γ-ray detector),

-electro-optic modulators,

-nonlinear optical devices,

-room-temperature x-ray detectors,

-optical elements for infrared application.

For several years the polycrystalline thin-film CdTe/CdS solar cell has been considered to be a promising alternative to the more widely used silicon devices [9]. It has several properties that make it especially attractive:

i. The cost of CdTe solar cells from polycrystalline materials and glass is potentially much cheaper than bulk silicon.

ii. The bandgap of CdTe is ideal for solar cell application because it matches the sunlight spectrum very well.

iii. Thin-films can be prepared using a variety of different techniques due to the chemical and physical properties of the semiconductors.

iv. The absorption coefficient of CdTe is very high so that approximately 99% of the incident light can be absorbed by a layer thickness of only 1μm (compared with around 10μm for Si), which decreases the quantity of semiconductor required in the applications.

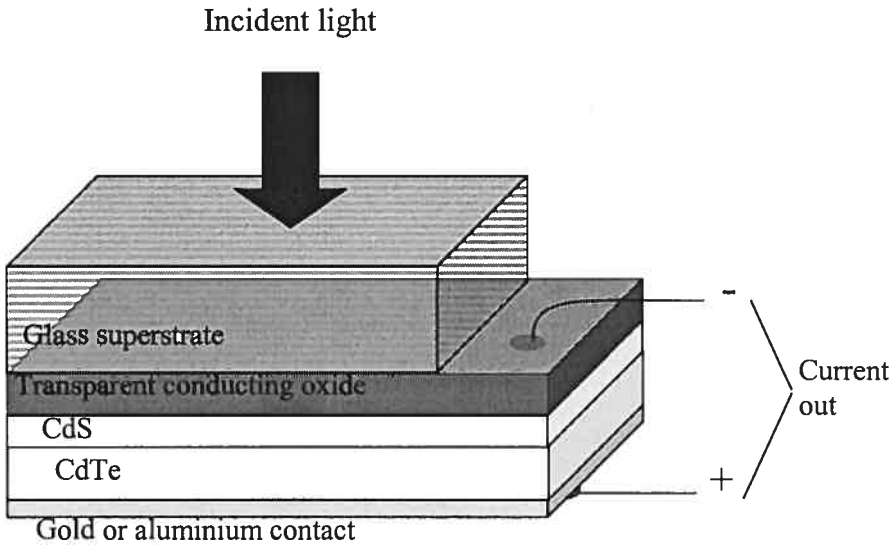

Figure 1.1, A typital CdS/CdTe solar cell structure (not to scale). The CdTe/CdS solar cell is based upon the heterojunction formed between n-type CdS and p-type CdTe. Glass substrate protects the active layers and offers the window layer. Transparent conducting oxide acts as the front contact and the window layer to the device. CdS layer provides one half of the p-n junction and the window layer. CdTe layer is the active region of the solar cell and the active junction is formed at the interface between n-type CdS layer and p-type CdTe layer. Gold or aluminium is the back contact [10].

Furthermore, CdTe/CdZnTe (CZT) based γ-Ray detectors have been developed intensively and have recently seen significant improvements [11]. These detectors are mainly used in the nuclear industry and nuclear medicine. CZT detectors have high resistivity because of the wide bandgap and also have high photon absorption efficiencies because of the large atomic number Z and high density. In addition, CZT detectors show low noise at room temperature due to their high resistivity.

To obtain high-quality photoelectric devices with high efficiency, the semiconductor materials must have high purity. Thus, a more detailed physical understanding of the effect of defects and impurities upon device applications seems to be essential for further progress [12]. For example, R. Benzaquen has reported a temperature dependence of shallow-donor bound-exciton-emission linewidths and exciton-impurities interactions in high-purity InP in detail [13-14], and E. S. Koteles has extensively investigated high-purity GaAs [15]. For these reasons considerable effort has been spent in growing pure and defect-free high quality CdTe crystals. Numerous studies on CdTe have also been made on crystal growth and photoluminescence (PL) properties with respect to various shallow acceptor- and donor-impurity complexes in the past few decades and many papers have focused on the PL spectra of CdTe, most being directed toward identifying impurities and defects responsible for the various spectral features [16-20]. Therefore it is also important to investigate the basic dynamical properties of bound exciton in high-purity CdTe as a function of sample growth and application parameters.

1.2 Bound excitons in semiconductors

Since most semiconductor materials contain significant amounts of impurities and/or defects which can trap excitons, the identification of the bound exciton states provides an important characterization of impurities, which control the electro-optic properties of semiconductors.

In high purity and high quality semiconductors at low temperature, the Coulomb attraction between electrons and holes causes their motion to be correlated and results in electron-hole pairs, known as excitons. Similar to the way that free carriers can be bound to (point-) defects, when the sample contains a small number of donors or acceptors (or defects), the excitons can also be bound to these impurities (or defects) via van der Waals interactions [21]. These are known as bound excitons (BE): neutral-acceptor-bound exciton (commonly abbreviated as $\left(A^0, X\right)$), ionized-acceptor-bound exciton (to be abbreviated as $\left(A^-, X\right)$), neutral-donor-bound exciton (abbreviated as $\left(D^0, X\right)$) and ionized-donor-bound exciton (abbreviated as $\left(D^+, X\right)$).

Bound excitons give rise to photoluminescence emission at lower energy than that of free excitons. The binding energy E^b of an exciton to the complex is defined as the energetic distance from the lowest free exciton state at $k=0$ to the energy of the bound state of the exciton.

The spectral positions of the principal excitonic lines usually can be estimated from the following expressions [24]:

$$E_{(D^0,X)} = E_g - (E_X + \xi E_D) \quad (1)$$

$$E_{(D^+,X)} = E_g - (E_D + \xi E_D), \quad (2)$$

$$E_{(A^0,X)} = E_g - (E_A + \xi E_A), \quad (3)$$

$E_{(D^0,X)}$, $E_{(D^+,X)}$, and, $E_{(A^0,X)}$, respectively, express the spectral positions of (D^0,X), (D^+,X) and (A^0,X). E_g and E_X are the band-gap energy and the binding energy of free exciton. E_D and E_A are the ionization energies of donor and acceptor impurities. ξ is the localization coefficient of the free exciton. In silicon, first observed by Haynes, ξ has a value around 0.1 [21, 22, 46]. However, the neutral donors and neutral acceptors have different behaviors in CdTe. Donor bound excitons (DBE) follow ξ =0.2 and many acceptor-bound excitons follow ξ=0.1 [23]. The binding energy of free exciton to complex can also be obtained from the optical spectra containing much more detailed information. The binding energies and emission peaks for several different donor- and acceptor-bound excitons and the ionization energies of several donor and acceptor impurities are listed in Table I.

At low temperature the near-band-edge photoluminescence (and absorption) spectra of semiconductor materials (such as direct gap III-V and II-VI semiconductors) is usually dominated by the narrow bound-exciton emission lines. High attention is concentrated on these lines since they are extremely useful for impurity characterization in these materials. Figure 1.2

Table I PL energies of bound-exciton recombinations in CdTe [25-26]. PL energies of bound-exciton recombinations are listed at the second column. E^b is the binding energy for exciton bound to donor or bound to acceptor. E_D and E_A are ionization energies of donor and acceptor, respectively.

Donor	(D^0, X) (eV)	E^b (meV)	E_D (meV)
F	1.59314	3.36	13.67
Ga	1.59309	3.41	13.88
Al	1.59305	3.46	14.05
In	1.59302	3.48	14.15
Cl	1.59296	3.54	14.48
---	1.59284	3.66	14.60
I	1.5927	3.8	~15.1
Acceptor	(A^0,X) (eV)	E^b (meV)	E_A (meV)
O	---	---	46
N	1.5892	7.2	56.0
Li	1.58923	7.17	58.0
Na	1.58916	7.24	58.7
Sb	1.5895	6.8	65
P	1.58897	7.43	68.2
As	1.58970	6.70	92.0
Ag	1.58848	7.92	107.5
Cu	1.58956	6.84	146.0
Au	1.57606	20.34	263

shows a typical photoluminescence spectrum of an n-type InP at low temperature. Recombination peaks such as $(F,X)_{n=1}$, $(D^0,X)_n$, (A^0,X) and so on are well identified in figure 1.2.

A paper by R. Benzaquen *et al* (1995) presented a temperature-dependent PL spectroscopy study of the neutral shallow-donor bound-exciton emission in a high-purity, n-type InP [14]. By a simple formula based on the model of a two-step dissociation mechanism, R. Benzaquen analyzed in detail the temperature dependence of the PL integrated intensities of two components of the shallow-donor bound-exciton transitions ($(D^0,X)_{n=1,2}$) and revealed the presence of two dissociation channels:

(1). $(D^0,X)_{n=1,2} \rightarrow D^0 + X$.

(2). $(D^0,X)_{n=1,2} \rightarrow D^0 + e + h$.

The dissociation channel (1) results in the liberation of a free exciton from a shallow neutral donor with activation energy E_{T1} equal to the binding energy E^b of the donor-bound exciton. The channel (2) describes the liberation of a free electron and a free hole from a shallow neutral donor with activation energy $E_{T2} = E^b + E_X$. When the temperature is increased from 4.2 K to about 8 K, the dissociation channel (1) dominates the donor-bound-exciton transitions. When the temperature is further increased to 20 K, channel (2) becomes the dominant dissociation path. These results about the dynamics of donor-bound excitons in high-purity InP inspired us to make an effort to explore the dynamics of donor-bound excitons in high-purity CdTe semiconductor.

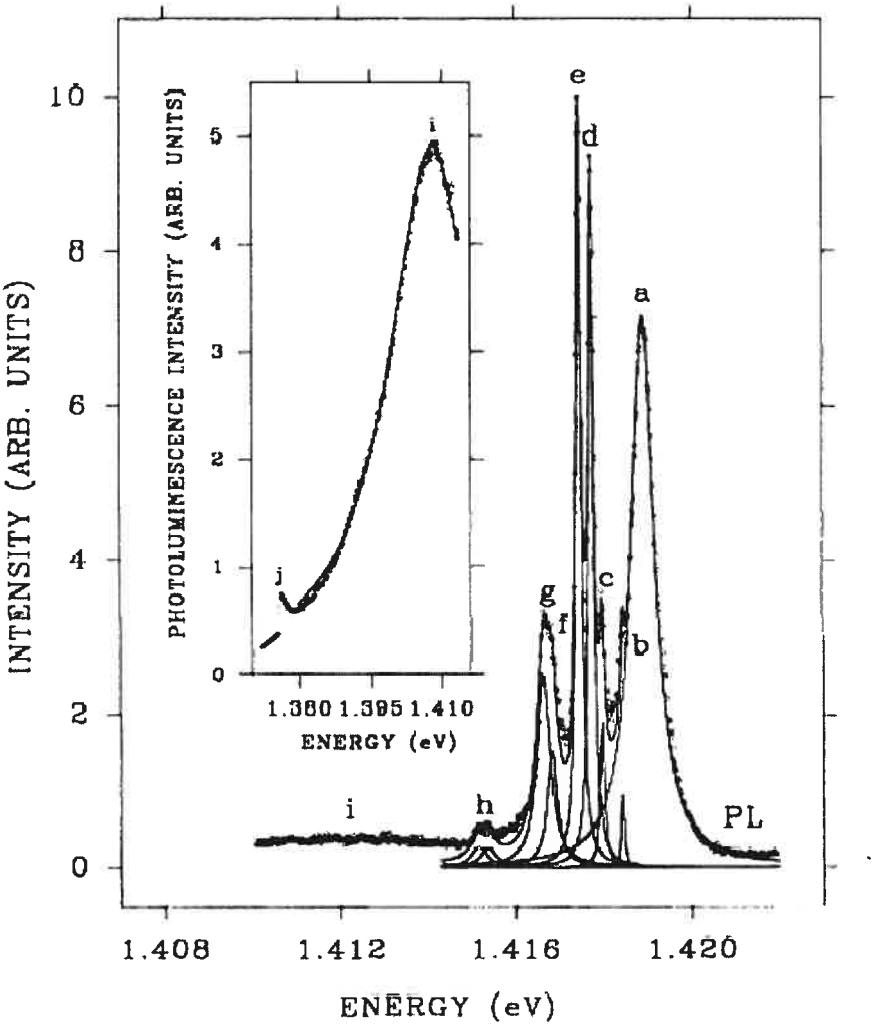

Figure 1.2 4.2-K photoluminescence (open circles) of n-type InP [27]. The solid curves are Lorentzian fits to the PL data. $a = (F,X)_{n=1}$ is the $n = 1$ free-exciton transition; *b, c, d*, and *e* are, respectively, the $n = 4$, 3, 2, and 1 neutral shallow donor bound-exciton transitions $(D^0,X)_n$; $f = (D^0,h)$ is the neutral shallow donor to free-hole recombination; $g = (D^+,X)$ is ionized donor bound-exciton transition; $h = (A^0,X)$ is the neutral acceptor bound-exciton transition; $i = (D_2^0,X)$ is the neutral deep-donor bound-exciton recombination; $j = (D^0,A^0)$ is the shallow donor-acceptor pair recombination.

1.3 About this mémoire

This work is concerned with the dynamics of donor-bound excitons in high-purity CdTe at low temperature between 1.8 K and 24 K, by analyzing the temperature dependence of the integrated photoluminescence intensity in detail. From the measurements of Fourier-transformed infrared photoluminescence spectra, photoluminescence emission and photoluminescence excitation spectra, we observe $(D^0, X)_n$ transitions, interpret the data with a two-step dissociation model and deduce the details of the dissociation processes. At the same time we obtain some physical parameters about donor-bound excitons in high-purity CdTe. All the works was done at laboratory G.C.M. (Group of Thin Films) of the Université de Montréal.

This mémoire consists of the following chapters. In Chapter 2, we review various basic concepts used in our work. We discuss the polariton concept and polariton dispersion relation in detail. We present Fano lineshape and Lorentzian equations, and introduce the activation energy associated with a two-step dissociation model to be used in our study.

In Chapter 3 we describe the experimental samples, experimental setups and measurement methods.

In Chapter 4 we present the optical characterization of some CdTe samples including Fourier-transformed infrared photoluminescence spectra,

photoluminescence and photoluminescence excitation spectra, at the low temperature.

In chapter 5 we analyze the temperature dependence of integrated PL intensity of high-purity CdTe sample and interpret experimental data in detail.

The results and conclusions of this work are briefly summarized in Chapter 6

CHAPTER 2

THEORY

Throughout this chapter, some of the important concepts and theories directly relevant to this work will be presented in detail. We first provide a review on exciton-polariton in direct-band-gap semiconductors due to the important relation between polaritons and luminescence spectra at low temperature. This review is based on the publications of D. Bimberg [28], R. Benzaquen [13-14] and D.E. Cooper [29]. After this review, we discuss the Lorentzian equation which describes the basic lineshape for a homogenous transition, and the Fano lineshape equation which is suited to fit the asymmetric lineshapes in the PL spectra of CdTe. In addition, a two-step dissociation model, which properly explains the temperature-dependent integrated PL intensity and dynamical properties of DBE in high-purity CdTe samples, is introduced.

2.1 Polariton

Toyozawa [30] pointed out for the first time that the luminescence spectra in semiconductors at low temperature should be interpreted in term of polaritons. Using the dispersion relation of exciton-polariton, R. Benazquen has presented exciton-impurities interactions in high-purity InP [14] and E. S. Koteles has thoroughly investigated high-purity GaAs [15].

In direct-band-gap semiconductors such as InP, GaAs and CdTe, exciton-photon strong interactions result in the formation of coupled modes called exciton-polaritons (to be abbreviated as polaritons in the latter part), which determine many optical properties of the semiconductors. The polariton dispersion curve for CdTe is shown in Figure 2.1, where the curves labelled I and II are usually referred to as the "upper" and "lower" branches of the polariton. The energy of the transverse exciton $E_T(k)$ is given by

$$E_T(k) = E_T + \frac{\hbar^2 k^2}{2M}, \qquad (4)$$

where k is the wave vector and M is the exciton mass. E_T is the zero-center transverse exciton energy. As a result of the coupling of pure exciton and photon states, the upper and lower polariton branches are formed, which can be described by a two-branch model (here we are only considering the dispersion relation of n =1 state) [14-15, 24, 31]:

$$\varepsilon(k,E) = \left[\frac{\hbar c k}{E}\right]^2 = \varepsilon_b\left[1 + \frac{2E_{LT}E_T^2(k)}{E_T(k)\left[E_T^2(k) - E^2\right]}\right], \quad (k \cdot E \neq 0) \qquad (5)$$

$$\varepsilon(k,E) = 0 = \varepsilon_b\left[1 + \frac{2E_{LT}E_T^2(k)}{E_T(k)\left[E_T^2(k) - E^2\right]}\right], \quad (k \cdot E = 0) \qquad (6)$$

$$E_{n,LT} = E_{n,L} - E_{n,T} = \left[\left(\frac{\varepsilon_b + 4\pi\beta}{\varepsilon_b}\right)^{1/2} - 1\right]E_{n,T}, \qquad (7)$$

Eqs. (5), (6), and (7), respectively, describe the dispersion relation of transverse

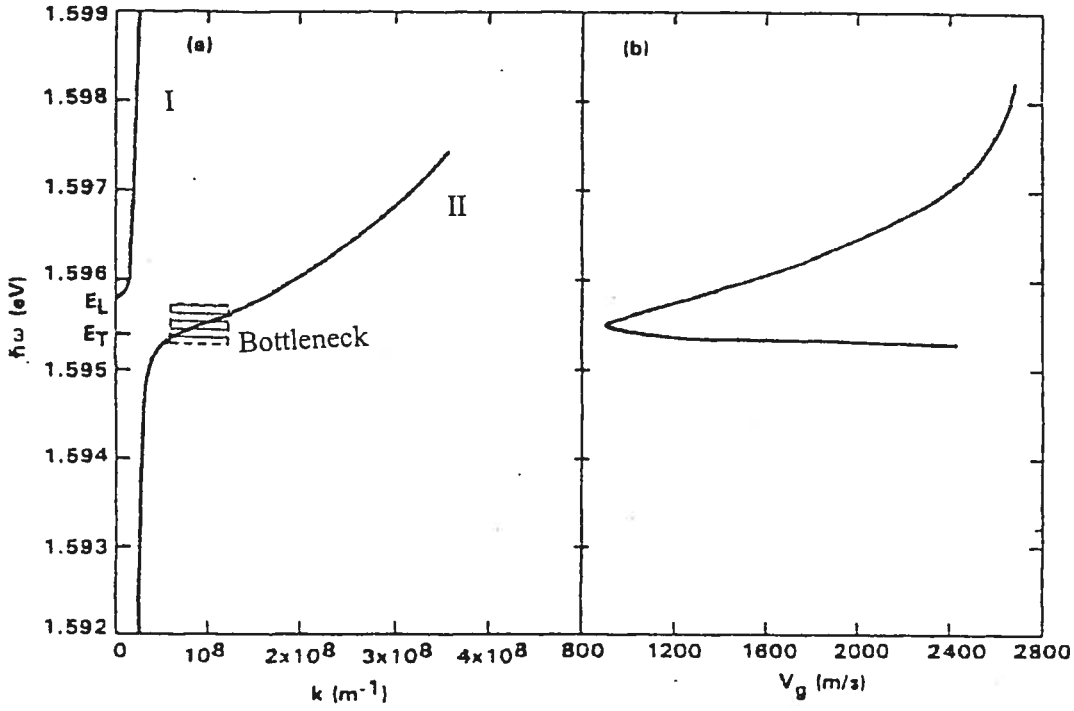

Figure 2.1 (a) Dispersion relation for excitonic polarions in CdTe, calculated with the polariton parameters given in Table I. The curve labeled I and II are usually referred to as the "upper" and "lower" branches of the polariton. (b) The polariton group velocity (v_g, bottom scale) on the lower branch as a function of polariton energy (left scale) (from [27]).

Table II Comparison of equivalent physical parameters of InP, GaAs, and CdTe [14, 29, 36]. m^* and m^*_{hh}, respectively, are the electron and heavy-hole masses, and ε_b and ε_∞ are, respectively, the low and high dielectric constants [37]. E_T is the n = 1 transverse exciton energy and E_X is the binding energy of free exciton . E_g is band gap. E_{LT} is the longitudinal-transverse exciton splitting energy at $k = 0$.

	InP	GaAs	CdTe
m^* (a.u.)	$0.082m_0$	$0.067m_0$	$0.096m_0$
m^*_{hh} (a.u.)	$0.85m_0$	$0.64m_0$	$0.81m_0$
E_T (eV)	1.4185	1.5153	1.5954
E_g (eV)	1.424 (16K)	1.519 (0K)	1.607 (10K)
E_X (meV)	4.82	4.2	10.5
ϵ_b	12.38	12.8	10.4
ϵ_∞	9.55	10.86	7.1
E_{LT} (meV)	0.13	0.13	0.65

polariton, longitudinal polariton and longitudinal-transverse exciton splitting energy. $\varepsilon(k,E)$, c, and E are, respectively, the dielectric function of the medium including the polariton contribution, the speed of light in vaccum, and the polariton energy. β is the exciton polarizability, and ε_b is the background dielectric constant excluding the polariton contribution. E_L is the longitudinal exciton energy. E_{LT} represents the longitudinal-transverse exciton splitting energy at $k = 0$ which gives a measurement of the coupling strength between the uncoupled longitudinal and transverse excitons at $k = 0$. It is to be noted that only the transverse excitons can interact with the electromagnetic field.

Polariton effects can be observed experimentally through reflectivity, transmission, and luminescence spectroscopy [32], and with particular success by Raman spectroscopy [33]. The emission of a photon by a polariton is fundamentally different from corresponding processes associated with most excited states, since electromagnetic energy resonant with the polariton band travels through the crystal as a polariton. Thus in order for a polariton in the interior of a crystal to emit as a photon, it must first migrate to the crystal surface, where it can be converted to a photon and thus radiated out from the crystal.

The polariton dispersion curve appropriate for CdTe (n=1) is presented in figure 2.1 (a). Figure 2.1 (b) displays the polariton group velocity on the lower polariton branch as a function of energy, which is related to the derivative of the polariton dispersion curve for the lower polariton branch. On the upper polariton branch (abbreviated as UPB) of the polariton dispersion curve, the polaritons

start out exciton-like at energy E_L and quickly become photon-like with increasing wave vector. On the lower polariton branch (LPB), at the large wave vector, the polaritons are predominantly exciton-like, whereas, at small wave vectors they are photon-like below energy E_T. The nature of the polariton dispersion relation has a profound effect on the luminescence mechanism in this energy region [29, 33]. For example, the lower-branch polaritons may be scattered by phonons into the energy region below or near E_T where radiative decay of polaritons can take place through their photon components. Furthermore, it has been shown that polariton-impurity scattering has a marked effect on the polariton luminescence line shape [34]. As the polariton relaxes toward the "knee" region of dispersion curve (Figure 2.1 (a)), the rate of photon emission decreases, forming a "bottleneck" [15, 35] which allows the polariton population to reach a thermal equilibrium with the crystal temperature, where the lifetimes of polaritons are the longest. As shown in Figure 2.1 (b), the group velocity of the lower-branch polaritons, $v_{LPB} = \hbar^{-1} dE_{LPB} / dk$, varies very rapidly with energy, and has a minimum just above the bottleneck (Figure 2.1 (b)). Velocity-dependent scattering processes are greatly enhanced in this energy region. This enhancement in scattering together with the low group velocity results in much slower diffusion of these polaritons. These phonon scattering rates decrease as polaritons below E_T become more photon-like, and on the other hand, polaritons are short-lived because they have high group velocity. The existence of a propagating mode such as the polariton in the crystal has a profound effect upon the

photoluminescence (PL) process, which must be viewed within the framework of a transport problem. Instead of a population of free excitons, which can recombine anywhere in the crystal producing photons that are free to excite the crystal unhindered, there is a population of polaritons that can produce external PL if the excitation first travels to the surface. In the polariton picture, a polariton impinging on the crystal interface has a certain probability of being transmitted and a certain probability of being reflected back.

2.2 Lorentzian and Fano lineshape equations

In this section we mainly introduce two lineshape equations, Lorentzian and Fano lineshape equations. They fit well DBE lines in the PL spectra of CdTe.

A) Lorentzian function

The Lorentzian function is the singly peaked function given by

$$I(E) = \frac{I_i}{1 + (\frac{E - E_f}{\sigma})^2}, \qquad (8)$$

$I(E)$: intensity at energy E

I_i: intensity of ith peak (maximum value at $E = E_f$)

E: energy position

E_f: center energy of peak (transition energy)

σ: half width at half maximum (HWHM)

The Lorentzian line shape is symmetric about its central energy E_f of the peak with a HWHM σ. E_f and σ will be treated as free parameters of the fit. The Lorentzian lineshape is a typical lineshape for homogeneously broadening optical transitions..

B) Fano lineshape equation

Fano interference is an universal phenomenon in physics which can be observed in various systems such as rare gases spectra, photodissoziation, bulk GaAs in magnetic field, superlattice in electric field, impurity ions in semiconductors, electron-phonon

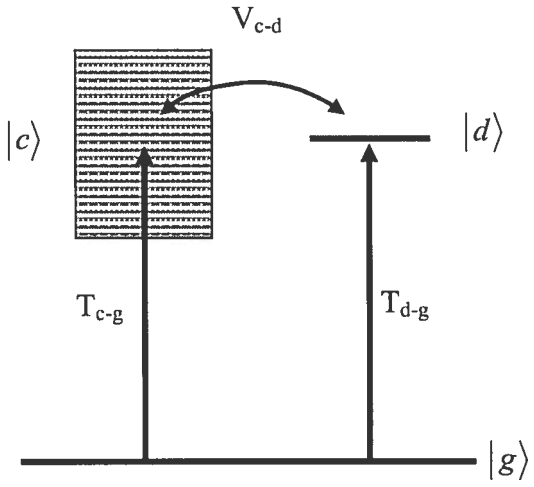

Figure 2.2 Energy scheme of a Fano interference system: A discrete state |d> and continuum |c> are coupled by an interaction V. The transition from a common ground state $|g\rangle$ to the discrete and continuous states leads to the typical lineshape.

coupling and many more [38-42]. In general, this interference arises by an interaction of a discrete state with an energetically degenerate continuum of states. The energy scheme of a Fano interference system is drawn in Figure 2.2. Excitation can take place from ground state $|g\rangle$ either into a discrete state $|d\rangle$ or into continuum state $|c\rangle$, corresponding to excitation path $T_{d\text{-}g}$ and $T_{c\text{-}g}$. The coupling manifests itself due to quantum mechanical interference $V_{c\text{-}d}$ between discrete state $|d\rangle$ and continuum state $|c\rangle$.

The equation of Fano lineshipe is given by [43- 44]:

$$I(\varepsilon) = \frac{(q+\varepsilon)^2}{(1+\varepsilon^2)} \quad , \qquad (9)$$

q: lineshape parameter

ε: the reduced energy given by:

$$\varepsilon = \frac{2(E - E_f)}{\Gamma}, \qquad (10)$$

E: energy position

E_f: transition energy

Γ: the width of the spectral feature (FWHM)

Figure 2.3 shows Fano lineshapes for different values of q. The Fano lineshape equation shows an asymmetric line shape at the energy E of the peak with a FWHM Γ. q, E_f and Γ will be treated as free parameters of the fit. The sign of q

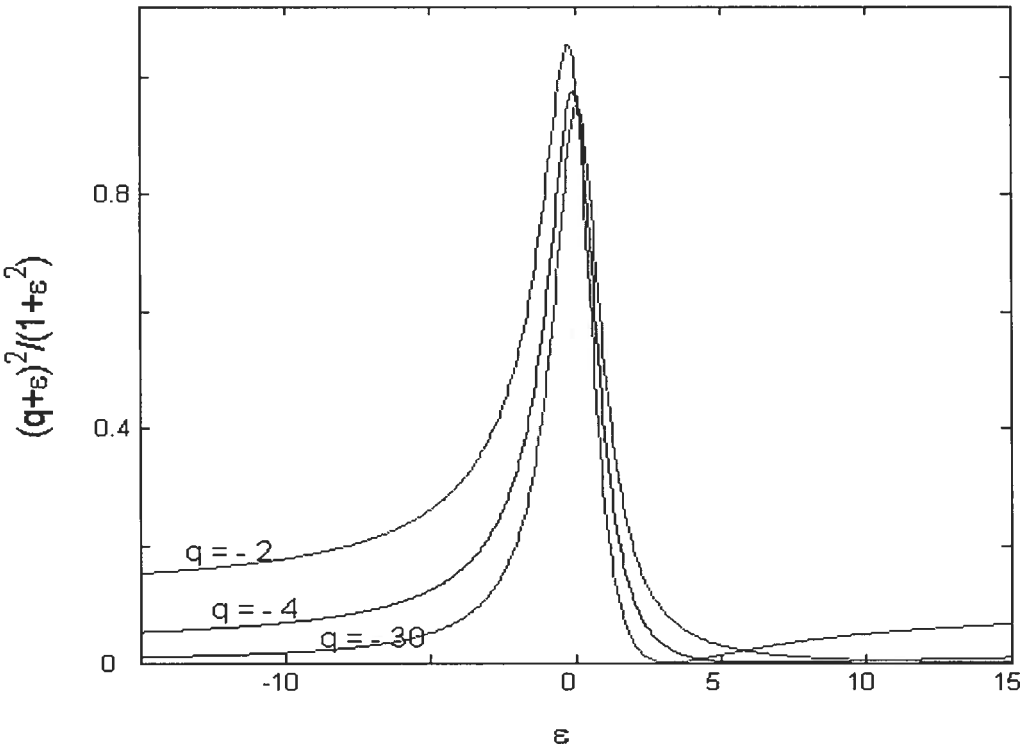

Figure 2.3 Natural line shapes for different values of q [43-44]. Reverse the scale of abscissas for positive q.

determines the asymmetry of the line due to interference effects. It is positive when the interaction is repulsive and negative when the electron-hole interaction is attractive. When $|q|$ is much greater than 1, Eq. (9) becomes equivalent to Eq. (8) in the region where the signal is the strongest.

We show a brief derivation for the simplest case of one discrete resonance and one continuum (the derivation follows S. Glutsch's "Exciton in Low-Dimensional Semiconductors") [45]. First, we start the derivation with Hamiltonian matrix element H and transition matrix element $|M\rangle$.

$$H = \begin{pmatrix} E_0 & V_1 & V_2 & \cdots \\ V_1^* & E_1 & 0 & \cdots \\ V_2^* & 0 & E_2 & \cdots \\ \vdots & \vdots & \vdots & \ddots \end{pmatrix}; \qquad |M\rangle = \begin{pmatrix} M_0 \\ M_1 \\ M_2 \\ \vdots \end{pmatrix}. \tag{11}$$

Where E_0 and E_l ($l > 0$ in the latter part of this section) are the energy of the discrete state and the energy of continuum. V_l, M_0 and M_l are, respectively, the coupling matrix element between the discrete state and the continuum, the transition matrix element to the discrete and transition matrix element to the continuum. The V_l and M_l can be expressed as

$$V_l = \frac{v(E_l)}{\sqrt{D(E_l)}}; \qquad M_l = \frac{\mu(E_l)}{\sqrt{D(E_l)}}, \tag{12}$$

where $D(E_l) = 1/(E_{l+1} - E_l)$ is the density of states.

The optical susceptibility was expressed as

$$\chi(\omega)=\sum_l \frac{\left|\langle M|\Phi_l\rangle\right|^2}{E_\Lambda-(\omega+i\in)}=\langle M|R(\omega+i\in)|M\rangle; \qquad (13)$$

$$R(z)=(H-z)^{-1};\ H|\Phi_l\rangle=E_\Lambda|\Phi_l\rangle;\ \langle\Phi_l|\Phi_{l'}\rangle=\delta_{ll'};\ \sum_l|\Phi_l\rangle\langle\Phi_l|=1.$$

Where $|\Phi_l\rangle$ is te normalized eigenvectors of H, and $\in=+0$ is a positive infinitesimal. ω is the resonance frequency. The function $R(z)$ is the resolvent and its matrix elements are the Green's function. With mathmetical relations it follows that

$$R_{00}(z)=\left[H_0-z-\sum_l{}'\frac{V_l^2}{E_l-z}\right]^{-1}$$

$$R_{l0}(z)=-\frac{V_l R_{00}(z)}{E_l-z};\quad R_{0m}(z)=-\frac{R_{00}(z)V_m}{E_m-z};\ m>0 \qquad (14)$$

$$R_{lm}(z)=\frac{\delta_{lm}}{E_l-z}+\frac{V_l R_{00}(z)V_m}{(E_l-z)(E_m-z)};\ l,\ m>0$$

Then the optical susceptibility is equal to:

$$\chi(\omega)=\left[M_0-\sum_l{}'\frac{M_l V_l}{E_l-(\omega+i\in)}\right]R_{00}(\omega+i\in)\left[M_0-\sum_m{}'\frac{V_m M_m}{E_m-(\omega+i\in)}\right]+\sum_l{}'\frac{M_l^2}{E_l-(\omega+i\in)}$$

For $D(E_l)\to\infty$, the following summation can be replaced be intergration on the right:

$$\sum_l{}'\frac{V_l^2}{E_l-(\omega+i\in)}=\int dE\,\frac{\nu^2(E)}{E-(\omega+i\in)}=F+\tfrac{1}{2}i\Gamma$$

$$\sum_l{}' \frac{M_l V_l}{E_l - (\omega + i\in)} = \int dE \frac{\nu(E)\mu(E)}{E - (\omega + i\in)} = G + \tfrac{1}{2} i\Delta \qquad (15)$$

$$\sum_l{}' \frac{M_l^2}{E_l - (\omega + i\in)} = \int dE \frac{\mu^2(E)}{E - (\omega + i\in)} = K + \tfrac{1}{2} i\Lambda$$

where F, G, K, Γ, Λ, and Δ are real numbers with

$$\Gamma = 2\pi\nu^2; \quad \Delta = 2\pi\nu\mu; \ \Lambda = 2\pi\mu^2 \text{ and } \Delta^2 = \Gamma\Lambda. \qquad (16)$$

With the above equations, the optical susceptibility becomes

$$\chi(\omega) = \frac{\left(M_0 - G - \frac{1}{2}\Delta\right)^2}{E_0 - F - (\omega + i\in) - \frac{1}{2} i\Gamma} + K + \tfrac{1}{2}\Lambda. \qquad (17)$$

The imaginary part of the optical susceptibility is the absorption coefficient α with

$$\alpha(\omega) = Im\,\chi(\omega);$$

$$\alpha(\infty) = Im\,\chi(\infty) = \tfrac{1}{2}\Lambda = \pi\mu^2, \qquad (18)$$

To avoid having a sum of a discrete resonance and a continuous background and obtain analytic function near real axis, assume that nontrivial case $\Gamma > 0$. Then let ω replace $\omega + i\in$ in eq. (17). We use the relation () to eliminate the parameter Γ in (). After some algebra using eq. (16), (17) and (18), the absorption equals to

$$\frac{\alpha(\omega)}{\alpha(\infty)} = \frac{Im\,\chi(\omega)}{\alpha(\infty)} = \frac{\left[E_0 - F - \omega - (M_0 - G)H/\Lambda\right]^2}{(E_0 - F - \omega)^2 + \frac{1}{4}\Delta^4/\Lambda^2}. \qquad (19)$$

Let

$$\varepsilon = \frac{\omega - E_0 - F}{\frac{1}{2}\Gamma} \; ; \qquad q = \frac{M_0 - G}{\frac{1}{2}\Delta} . \tag{20}$$

At last, get the famous Fano formula:

$$\frac{\alpha(\omega)}{\alpha(\infty)} = \frac{(q+\varepsilon)^2}{1+\varepsilon^2} , \tag{21}$$

2.3 Activation energy

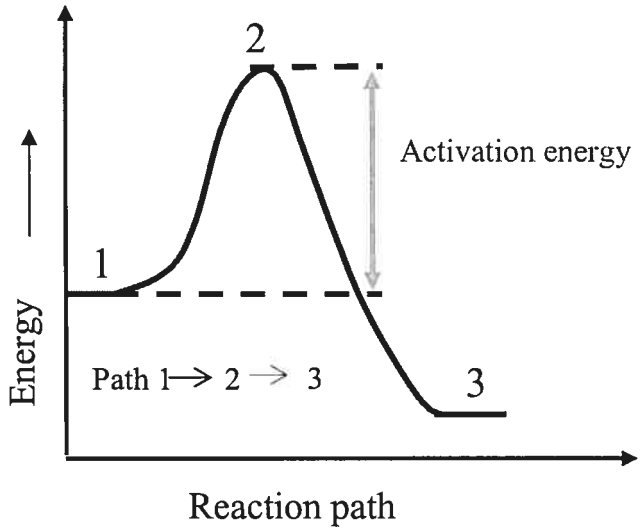

Figure 2.4 Schematic diagram of activation energy. Reaction path is 1 → 2 → 3.

Activation energy is defined as the energy that must be invested in a reaction to get it done. Figure 2.4 gives the schematic diagram of the relation of reaction path and

activation energy. If the reaction with the original state 1 and the end state 3 can happen, it must pass a medial sate 2.

R. Benzanquen analyzed the integrated PL intensities of DBE lines in high-purity InP using the following equation:

$$I^*_{(D^0,X)_{n=1,2,3}}(T) = \frac{I^*(0)}{1+\sum_{i=1}^{N} C_i exp[-(E_{t,i}/k_B T)]}, \qquad (22)$$

$I^*_{(D^0,X)_{n=1,2,3}}$: the temperature dependence of the integrated PL intensities

$I^*(0)$: the integrated PL intensity near 0 K

$E_{t,i}$: the ith activation energy

C_i: the ith constant linked to the degeneracy of $E_{t,i}$

This activation energy $E_{t,i}$ can often be related to the energy that is necessary to free an electron from a bound state.

To get equation (22), firstly, there are the following assumptions [13, 28]:

(1) The exciton complex has at least three states: ground-state energy E_0, where it is bound, and two higher states with energies E_1 and E_2, where they are dissociated. The two paths of dissociation have energies $E_{T1} = E_1 - E_0$ and $E_{T2} = E_2 - E_0$.

(2) Consider each electron-hole pair as a complete system and the rest of the crystal including all the other electron-hole pairs merely as a temperature bath. At the same time the pair-pair correlations are neglected.

(3) The three-level system is in thermal equilibrium at temperature T.

According to these assumptions the electron-hole pairs among the three levels are governed by the Boltzmann distribution. Then there are the following equations:

$$N_0(T)+N_1(T)+N_2(T)=N_G(T), \tag{23}$$

$$\frac{N_1(T)}{N_0(T)}=\frac{\alpha_1}{\alpha_0}e^{-\frac{(E_1-E_0)}{kT}}, \tag{24}$$

$$\frac{N_2(T)}{N_0(T)}=\frac{\alpha_2}{\alpha_0}e^{-\frac{(E_2-E_0)}{kT}}, \tag{25}$$

where, $N_0(T)$, $N_1(T)$, and $N_2(T)$ are the average numbers of bound excitons being in the levels E_0, E_1, and E_2 at the temperature T, respectively; α_0, α_1, and α_2 are the degeneracies of these levels. $N_G(T)$ expresses the total number of electron-hole pairs within the three levels at the temperature T.

Equations (23), (24) and (25) are combined to form another formula for $N_G(T)$:

$$N_G(T)=N_0(T)\left[1+\frac{\alpha_1}{\alpha_0}e^{-\frac{(E_1-E_0)}{kT}}+\frac{\alpha_2}{\alpha_0}e^{-\frac{(E_1-E_0)}{kT}}\right], \tag{26}$$

Here $N_G(T)$ is regarded as constant at the experimental temperature. Then we have $N_G(T) = N_G(0) = N_0(0)$. This assumption is consistent with the experiments as seen from the good fit of theory and experiment [22, 34]. Therefore from Eq. (26) we obtain:

$$\frac{N_0(T)}{N_0(0)} = \left(1 + C_1 e^{-\frac{E_{t,1}}{kT}} + C_2 e^{-\frac{E_{t,2}}{kT}}\right)^{-1}, \qquad (27)$$

where $c_1 = \alpha_1 / \alpha_0$, $C_2 = \alpha_2 / \alpha_0$, $E_{t,1} = E_1 - E_0$, $E_{t,2} = E_2 - E_0$.

If we don't consider any change in the radiative recombination probability with temperature, then $N_0(T)/N_G(T)$ can be exactly applied to the radiative recombination process with energy $\hbar\omega$. From Eq. (27) we get

$$I_T/I_0 = \left(1 + C_1 e^{-\frac{E_{t,1}}{kT}} + C_2 e^{-\frac{E_{t,2}}{kT}}\right)^{-1}. \qquad (28)$$

where the physical meaning of this equation is the ratio of the radiative intensity I_T at temperature T and the radiative intensity I_0 at 0 K when two activation processes are considered.

When N activation processes are taken into account, Eq. (28) is expressed as

$$I_T/I_0 = \frac{1}{1 + \sum_{i=1}^{N} C_i exp[-(E_{t,i}/k_B T)]}. \qquad (29)$$

CHAPTER 3

EXPERIMENTAL TECHNIQUE

3.1 Experimental samples

The various transition processes in semiconductors strongly depend on the temperature, the concentration of impurities, the intensity and wavelength of exciting light. In our case, a variety of cadmium telluride samples from various sources with different dopant were examined, and the CdTe sample with the greatest amount of donor-bound-exciton emissions was selected for our study. These samples include CdTe LAH, CdTe/Sb, CdTe/As, CdTe #1, and CdTe #18. CdTe LAH sample is a commercial sample doped with a little donor to compensate acceptors. CdTe/Sb sample contains about 130-ppm of Sb by weigh. CdTe/As sample is a CdTe sample doped with As of unknown concentration. CdTe # 1 and CdTe #18 are nominally pure CdTe samples. CdTe LAH sample was provided by Professor L. A. Hamel and the other CdTe samples were grown at laboratory of Université de Liège (Belgium).

Before the samples were mounted in the cryostat cooled by liquid helium to take the photoluminescence measurements, it was necessary to clean them in order to eliminate the impurities on the surface. For this purpose, the samples were

soaked in a 2% Br/CH_3OH solution for approximately five minutes, and then rinsed with a methanol solution [29].

3.2 Experimental setup

Photoluminescence (PL) is an important and the most common physical phenomena widely used to characterize semiconductors, which depicts a sample's energy structure while possibly revealing other important material features [47]. In brief, photons (commonly from a laser source), with energy E_{laser} greater than the bandgap E_g of the semiconductor sample studied, are directed onto the surface of the sample, and they are partially reflected, absorbed, and transmitted by the sample. The absorbed photons create electron-hole pairs by exciting electrons to the conduction band or to the energy states within the gap in the sample. Meanwhile, electrons can lose part of their energy and transfer from the conduction band to lower energy levels. PL occurs when photons, which are produced as a result of various recombinations events of electrons and holes, are emitted from the sample surface or the bulk. The emitted photon has a specific energy E_{PL} corresponding to the material's specific structure, composition and quality. The intensity and spectral content of the photoluminescence is also a direct measure of various important material properties.

PL spectroscopy is usually performed at low temperatures in order to obtain spectral resolution of different emission lines. Nevertheless, PL spectroscopy at room temperature has also received increasing interest, because room-temperature PL mapping of band-edge emission and deeper defect-related

emissions has proved to be a useful technique to characterize the homogeneity and crystalline quality of II-VI semiconductor materials.

Photoluminescence excitation (PLE) spectroscopy is another popular technique for studying thin epilayers grown on opaque bulk substrates, and it has been proved that PLE spectroscopy is very powerful to investigate excited states of bound-exciton complexes [48]. In brief, PLE is a technique that records the emission intensity of a particular photon energy from the samples as a function of the excitation photon energy. PLE spectra usually exhibit some resonance peaks, which indicate that the emission can be particularly strong excited at certain photon energies.

In the measurements of PL and PLE spectra of CdTe sample, the samples were mounted in the cryostat cooled by liquid helium at approximately 5K. To obtain steady-state PL spectra, the optical excitation comes from a tunable Ti:sapphire laser pumped by an Ar^+ laser with an output power maintained at 150 mW. The excitation light is focused on the sample by a convergent lens, and at the same time the PL collected by a set of lenses is dispersed by a 1-m double spectrometer with holographic gratings and then detected by a CCD camera cooled with liquid nitrogen, or by a GaAs photomultiplier cooled by the Peltier effect. For PL measurements, the spectrometer was centred at 7787 Å for DBE spectra, and for PLE, the Ar^+ laser was controlled by a feedback system adjusting the laser intensity in order to get constant intensity of the Ti-sapphire laser in the used wavelength range. During the experiment, additional measurements between 1.8 and 4.5 K were taken by immersing the sample in superfluid liquid helium (T < transform temperature 2.2 K). An attenuator with

transmission coefficient equal to 0.2% is inserted in order to reduce the laser power. The diagram of the experimental setup is shown in Figure 3.1.

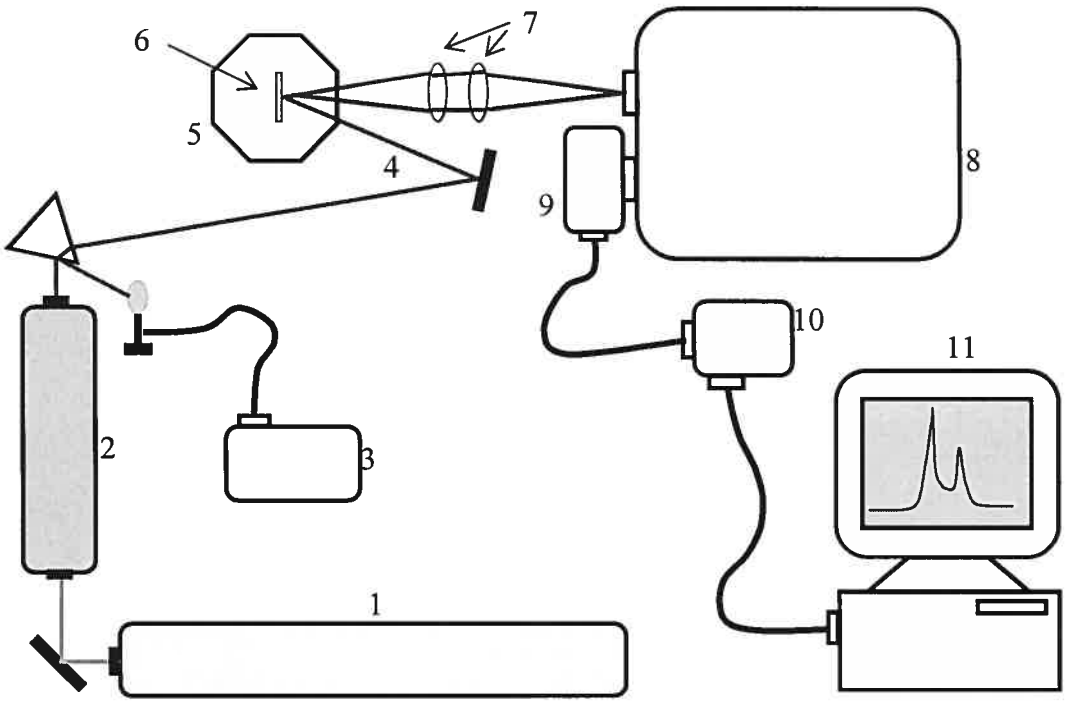

Figure 3.1 Schematic diagram of setup for PL and PLE (not drawn to scale and positions represented are approximate).

1. Argon laser
2. Ti-sapphire laser
3. Detector for stabilization of power with retroaction of the Ar^+ laser
4. Convergent lens
5. Cryostat
6. Sample
7. Sets of lenses
8. double spectrometer
9. Photomultiplicatorr GaAs/Camera CCD
10. photon counter
11. Computer (control and acquisition)

CHAPTER 4

OPTICAL CHARACTERIZATION OF CdTe SAMPLES

4.1 Low-resolution PL spectra

Prior to the high spectral resolution photoluminescence measurements, we took the measurements of low-resolution photoluminescence spectra of all samples in order to obtain the spectra more quickly. Low-resolution-photoluminescence (to be abbreviated as LRPL) measurements were performed with the samples in a He flow cryostat at the temperature of 5-8 K and using a BOMEM DA8 Fourier transform infrared spectrometer (abbreviated as FTIR). FTIR spectra can show the emission features in a large range of energy and allow the identifications of the emission lines.

Figure 4.1 and 4.2 display the FTIR photoluminescence spectra for all CdTe samples and single CdTe LAH sample, respectively, and the spectra were recorded at the same experimental conditions using a Si detector. It is observed that the CdTe LAH sample shows the sharpest (D^0, X) emission lines in figure 4.1 (see the inset of figure 4.1). Furthermore, the spectra of CdTe LAH, CdTe/As and CdTe/Sb samples also show very clearly the (A^0, X) emission lines. In the FTIR photoluminescence spectrum for single CdTe LAH sample (see figure 4.2), the sharp features associated with the emission lines of

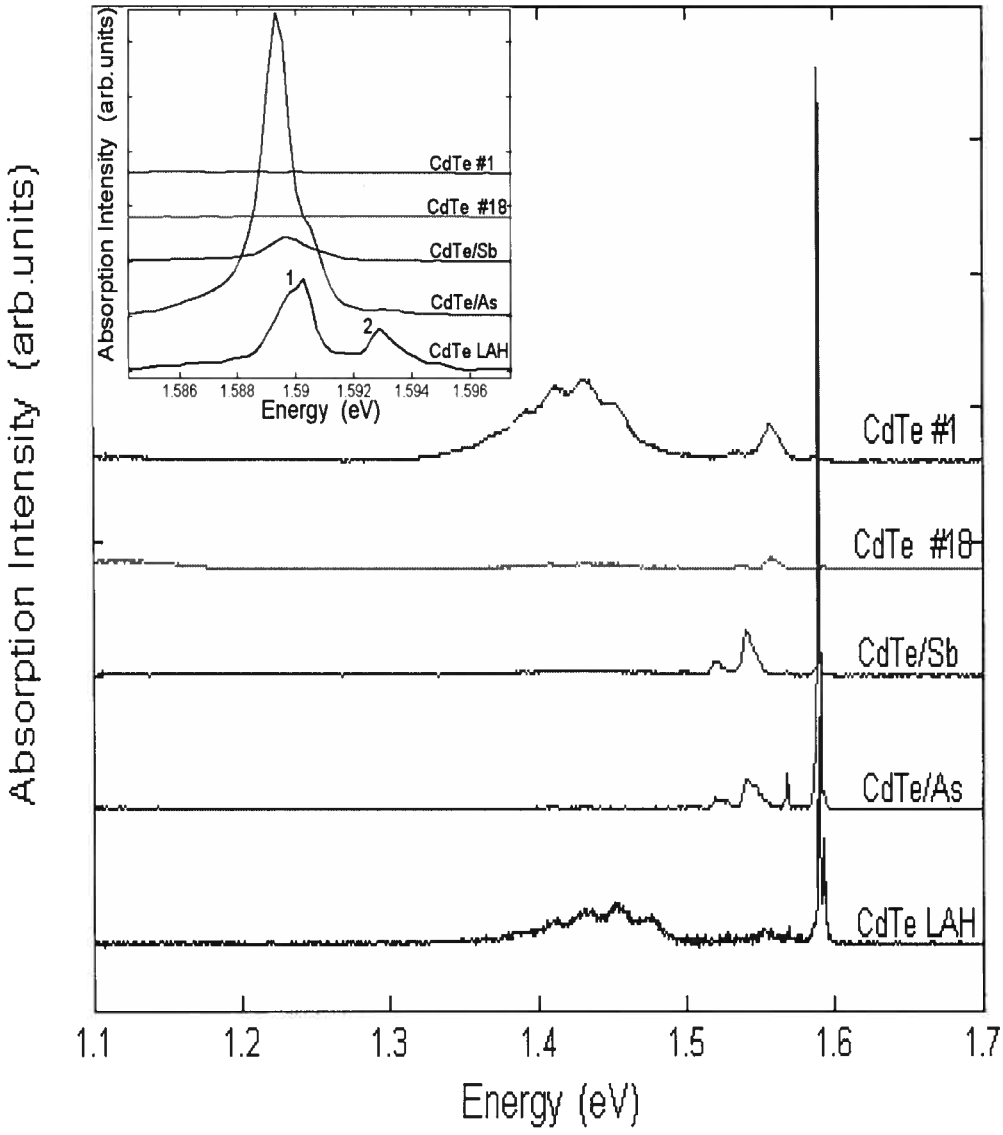

Figure 4.1 Low-temperature FTIR PL data for five samples at the same experimental conditions. The spectral features in inset labeled 1 and 2 are associated with $\left(A^0, X\right)$ and $\left(D^0, X\right)$ emission lines, respectively.

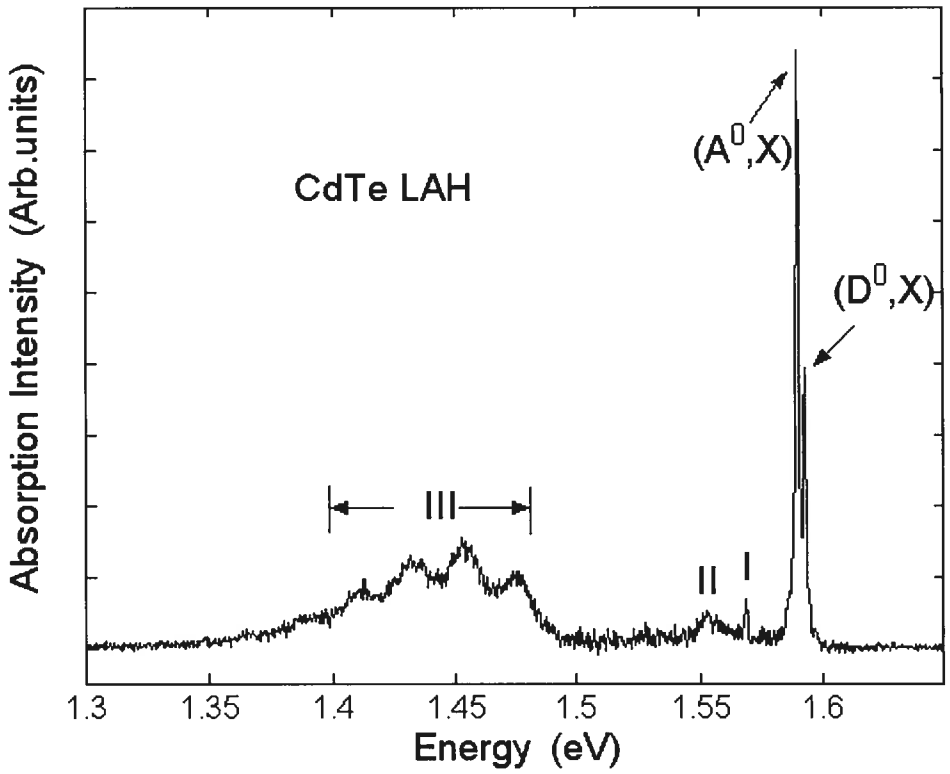

Figure 4.2 The FTIR PL spectrum for CdTe LAH sample at 8 K. The sharp features associated with (A^0, X) and (D^0, X) emission lines are clearly seen around 1.589eV and 1.593eV, respectively. The other labels are explained in the text.

(A^0,X) and (D^0,X) are clearly seen around 1.589 eV and 1.593 eV, respectively. The spectral feature labelled I, which appears ~21 meV below the (A^0,X) emission lines, is associated with the photon replica ((A^0,X)-LO); the feature labelled II is donor-acceptor pairs (to be abbreviated as DAP or (D^0,A^0)); and the spectral features labelled III near 1.4 eV band are associated with the native defect complexes which are very important for the applications of CdTe semiconductors. In figure 4.1 we can note that the emission lines of native defect complexes are also present in the FTIR PL spectrum of CdTe #1 sample and that the spectra of CdTe/As, CdTe/Sb, CdTe #18 samples hardly show this feature. (A^0,X)-LO and (D^0,A^0) lines can also be strongly, or weakly seen in the spectrum of other samples.

As seen in the previous part of this section the five samples have different FTIR PL features at the low temperature and CdTe LAH sample shows not only the emission lines of (D^0,X) but other important features such as (A^0,X)-LO, DAP and native defect complexes. Our goal was to find a CdTe sample with highest purity. We especially rely on the emission lines of (D^0,X) which are much sharper in CdTe LAH sample than the other ones. We thus selected this sample to proceed to the study of the dynamics of (D^0,X).

4.2 PL and PLE spectra

We took the PL spectrum of the CdTe sample at 1.8K with the condition that the spectrometer was centred at 7787 Å in order to obtain clear and exact $(D^0,X)_{n=1,2,3}$ peaks. Figure 4.2 displays the $(D^0,X)_{n=1,2,3}$ transitions in the region between 1.592-1.595 eV at 1.8K. $(D^0,X)_{n=1,2,3}$ transitions have Fano lineshape fits (see APPENDIX II about the fitting parameters).

Virtual excitation or transition in spectrum means the creation of a state with the same wave function as the excited state, but with an energy which is different from the eigenenergy of this excited state. Any transition which has a finite lifetime has an energy which can be written according to the uncertainty principle of quantum mechanics as

$$\Delta E \times \Delta t \approx \hbar . \qquad (30)$$

Where, ΔE is the lifetime broadening, i.e., the spectral energy of full width at half maximum. Δt is the radiative recombination lifetime of the donor bound exciton. $\hbar$ is the ratio of Plank constant h to 2π.

The radiative recombination lifetime of the free exciton is in the nanosecond range [29]. In the spectrum of Figure 4.3, the values of the lifetime broadening for $(D^0,X)_{n=1,2,3}$ states are, respectively, 0.11meV, 0.16meV, and 0.10meV, which approximately correspond to the radiative recombination lifetimes of the donor-bound excitons on the order of picosecond (6.0ps, 4.1ps, and 6.6ps) according to uncertainly principle of equation (30). The radiative recombination lifetime of the donor-bound exciton in CdTe is thus shorter than that of the free

exciton. This is in agreement with homogeneous broadening of the donor-bound exciton.

In addition, PLE measurement of CdTe sample was taken in order to know well the spectral features at energies of interest to our studies. Figure 4.4 shows a PLE spectrum of CdTe sample monitoring the emission at 1.5904eV at 7.8 K. For comparison, the PL spectrum is shown along with the PLE spectrum at the same temperature. In the PLE spectrum at energies of interest in our study, we are able to identify the three strongly excited spectral features labelled a, b and c, which are associated with the $(D^0, X)_{n=1,2,3}$ peaks in the PL spectrum. The feature peaks exhibited in the PLE spectrum are near 1.5927eV, 1.5932eV, and 1.5938eV. The PLE spectrum is surprising since the presence of $(D^0, X)_{n=1,2,3}$ features is not expected in the excitation spectrum of ABE (acceptor-bound excitons). It has been mentioned that the $(D^0, X)_n$ lifetime broadening is around 6 ps. This might indicate that the binding lifetime of excitons to donors is so short that the excitons are liable to get free from the donors. The most possible reason for the present of $(D^0, X)_{n=1,2,3}$ peaks in the PLE spectrum of ABE is that free and bound excitons are constantly converted each in the other.

In order to further examine this hypothesis, the next chapter is focussed on studying the temperature dependence of the PL in details.

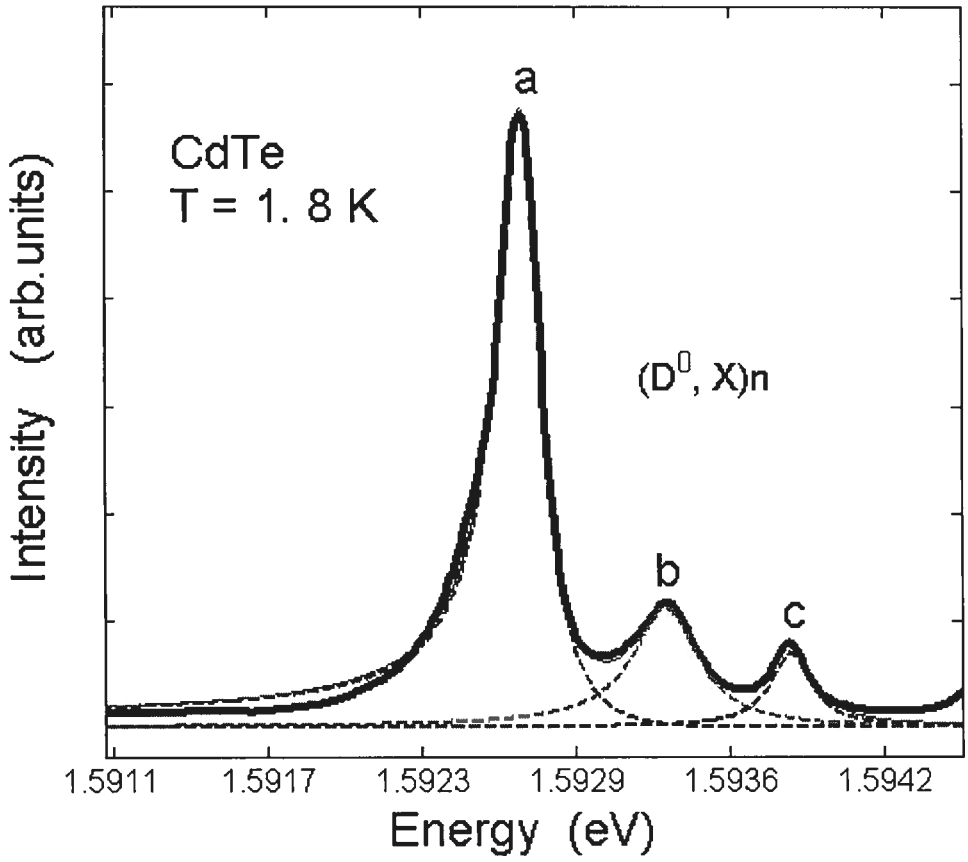

Figure 4.3 Temperature-dependent Photoluminescence spectra DBE of sample CdTe at T = 1.8 K. The spectrometer was centred at 7787 Å for DBE spectra. The dashed curves corresponding with a, b, and c, respectively, represent donor-bound-exciton transitions $(D^0,X)_{n=1,2,3}$ with Fano lineshape fits.

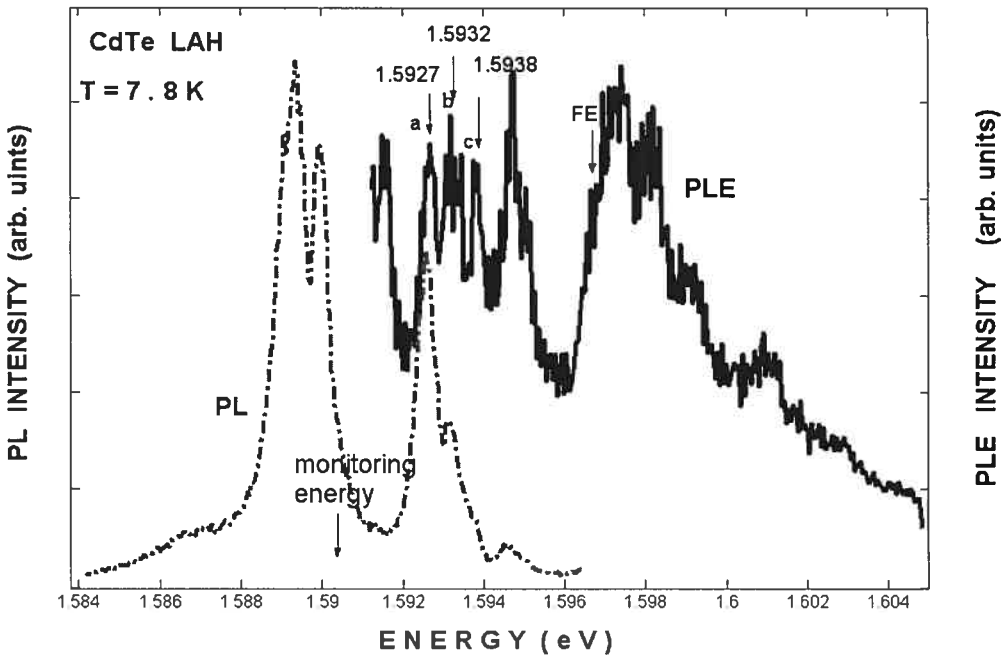

Figure 4.4, Photoluminescence (PL) and Photoluminescence excitation (PLE) spectra of CdTe sample recorded at 7.8 K for a detection of $(D^0, X)_n$ peaks labelled a, b and c. FE is free exciton peak. The dashed line and solid line are, respectively, PL and PLE.

CHAPTER 5

TEMPERATURE-DEPENDENT PL STUDIES

The temperature-dependent PL spectra of CdTe LAH sample were measured as a function of increasing temperature from 1.8 to 24.0K (keeping all other parameters constant). Figure 5.1 shows the temperature-dependent PL spectra of the CdTe sample observed at five different temperatures (respectively, 4.4K, 8.8K, 14.3K, 22.6K and 24.0K).

Three nice, clearly resolved $(D^0, X)_{n=1,2,3}$ transitions at 1.5927eV, 1,5933eV, and1.5938eV can be observed at low temperature. The intensity of the DBE line decreases with increasing temperatures and becomes very weak at 24 K. The line shapes of $(D^0, X)_{n=1,2,3}$ transitions are asymmetric, with the low-energy side broader than the high-energy side. These asymmetric peaks can be well fitted with Fano lineshapes using equation (9) (see APPENDIX II about all parameters of Fano fits).

In fact, while modeling the transitions, we experienced a great difficulty to fit the asymmetric $(D^0, X)_n$ transitions in the low energy region with the low-energy side broader than the high-energy side. To get an ideal fitting curve, we have tested several asymmetric distribution functions such as Gumbel, Genlogistic,

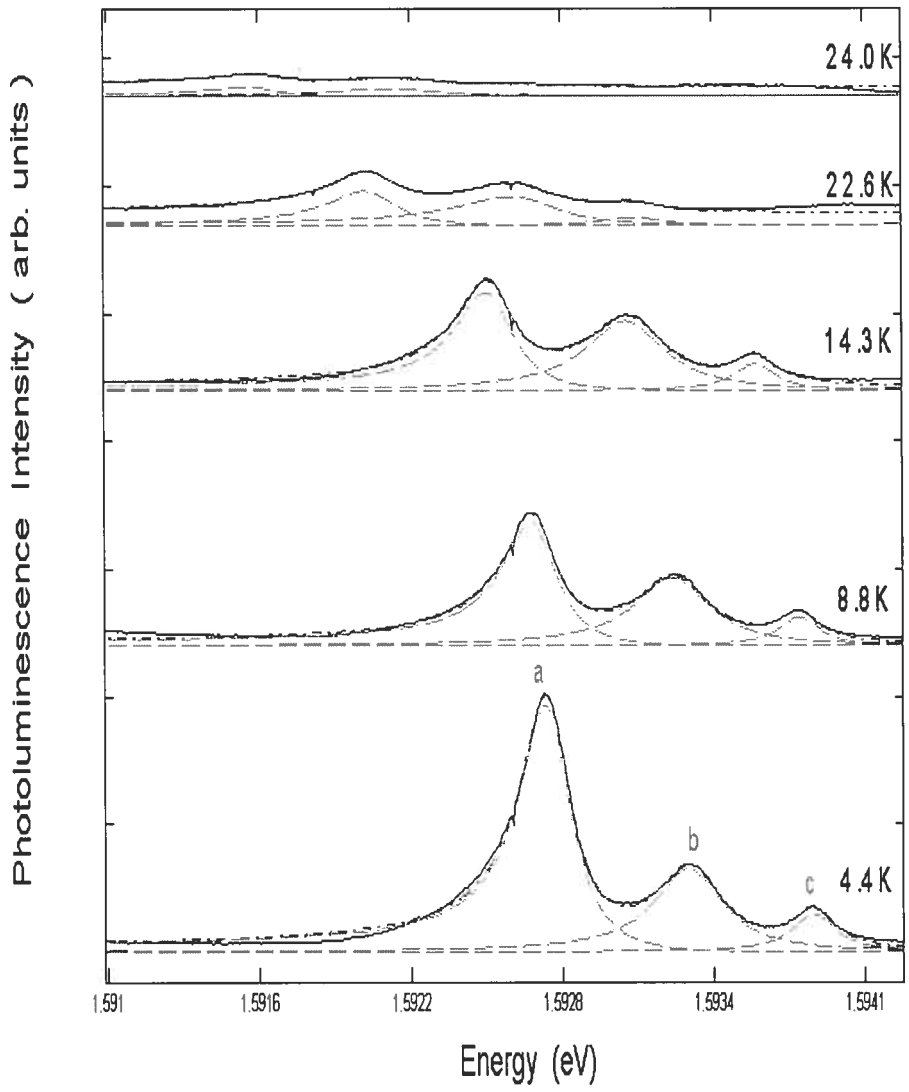

Figure 5.1 Temperature-dependent PL spectra of CdTe measured at several different temperatures, as indicated on the graph. The peaks labelled by *a*, *b*, and, *c*, respectively, are n = 1-3 components of donor bound-exciton transitions $\left(D^0, X\right)_n$. The dashed curves are Fano lineshape fits to the relevant transitions.

Fisk, Weibull and Lsqdlrtz lineshapes. In no case the asymmetric peaks agreed with these tested asymmetric functions. At last, the Fano lineshape function was found to be the closest to our ideal model. It is very interesting that the fitted curve of DBE asymmetric transitions agree well with Fano lineshape (see peak *a* in Figure 4.3) although it is not exactly Fano interference [38-39]. Finally, attention may be paid to interpreting the sign of the parameter q, which is certainly negative because the peak in Figure 5.1 sharply slopes on the high-energy shoulder. At the same time the value of small $|q|$ (between about 3-9) for the $\left(D^0,X\right)_{n=1}$ (i.e., peak a at 1.5927eV) displays the transition of pure and simple Fano lineshape, and then the very large $|q|$ (between about 25-170) of the $\left(D^0,X\right)_{n=2,3}$ (i.e., peak b at 1.5933eV and peak c at 1.5938eV) indicates approximate Lorentzian lineshapes with homogeneous energy broadening written as Eq. (8).

In analyzing the temperature-dependent integrated PL intensity, we use equation (11) to fit the data for $I^*_{(D^0,X)_{n=1,2,3}}$. When $N = 1$, using this equation to fit the value of C_i and $E_{t,1}$ fails to reproduce the data at the experimental temperatures. We got approximate good fits using this equation with $N = 2$ except that the experimental points don't agree very well with the fitting points in the region of 4-5 K, probably due to laser fluctuations. Figure 5.2 shows the temperature dependence of the integrated PL intensities $I^*_{(D^0,X)_{n=1,2,3}}$ versus $1/T$ in a logarithmic plot. The integrated PL intensities $I^*_{(D^0,X)_{n=1,2,3}}$ are calculated

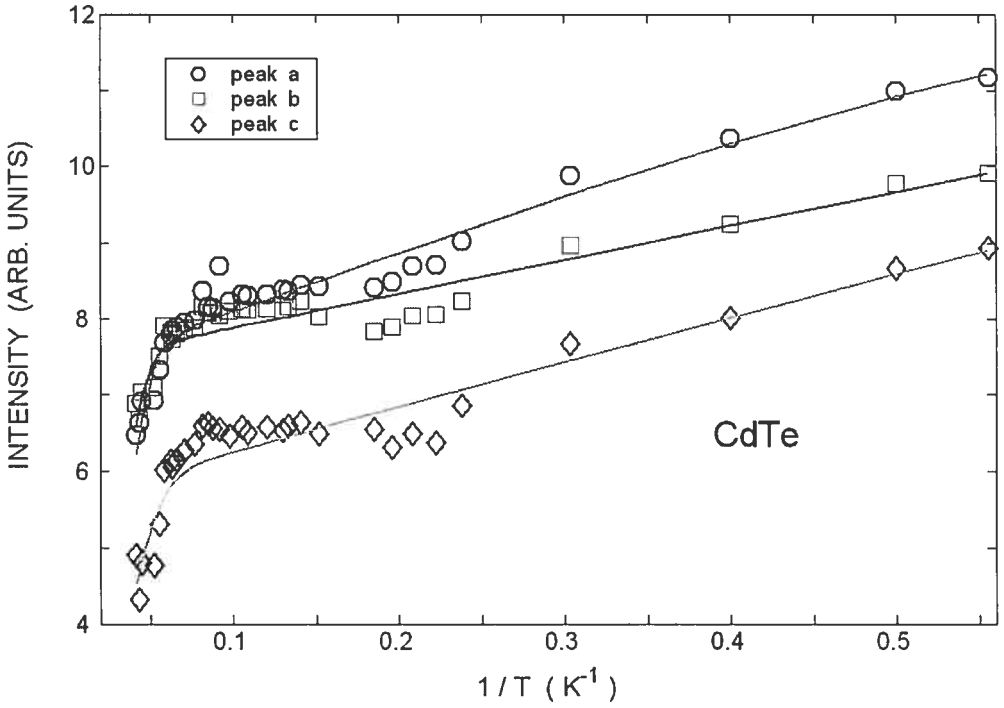

Figure 5.2 Temperature dependence of the PL intensities of structures a, b, and, c of Figure 8 in a ln(I) plot. Circles, square and diamonds are experimental points. The solid lines are the theoretical fits with two different dissociation energies derived from Eq. (29).

Table III. Parameters extracted from the analysis of integrated PL intensities of CdTe. $I^*(0)$ is the integrated PL intensity near 0 K, C_1 and C_2 are constants relative to $E_{t,1}$ and $E_{t,2}$ activation energies.

CdTe	peak a	peak b	peak c
$I^*(0)$ (10^3)	202.9(±105.4)	918.1(±0.02)	150.8(±0.01)
C_1	132.8(±57.0)	542.3(±43.2)	525.9(±56.1)
C_2 (10^3)	622.9(±0.3)	1722.9(±0.02)	213.3(±0.01)
$E_{t,1}$ (meV)	0.68(±0.06)	0.39(±0.02)	0.51(± 0.02)
$E_{t,2}$ (meV)	15.7(±1.5)	15.9(±0.9)	10.7(±0.7)

Table IV Parameters extracted from the experiment. Luminescence energies E_0 of $(D^0,X)_n$, energy $E_0 + E_{t,2}$, the bound energies E^b of $(D^0,X)_n$ and activation energies $E_{t,1}$ and $E_{t,2}$ from the fit parameters in CdTe samples are given in table.

CdTe Sample	E_0 (eV)	E_X+E^b (eV)	E^b (meV)	$E_{t,1}$ (meV)	$E_{t,2}$ (meV)
n=1	1.5927	14.2	3.7	0.68(±0.06)	15.7(±1.5)
n=2	1.5933	13.6	3.1	0.39(±0.02)	15.9(±0.9)
n=3	1.5938	13.1	2.6	0.51(± 0.02)	10.7(±0.7)

from CdTe sample of Figure 5.1, at the temperatures between 1.8 K and 24.0 K (see Table VI of APPENDIX III about $I^*_{(D^0,X)_{n=1,2,3}}$ at different temperature). All parameters extracted from fitting $I^*_{(D^0,X)_{n=1,2,3}}$ are shown in Table III. The solid line in Figure 5.2 is the "best-fit" to the data (circles, squares and diamonds) giving two activation energies $E_{t,1}$ and $E_{t,2}$, with $E_{t,1}$ and $E_{t,2}$ corresponding to the values of the slope at the regions of low and high temperature, respectively. Thus at low-temperature region (about 1.8-15K) the activation process is dominated by the dissociation process (or other energy-transfer path) with the lower activation energy $E_{t,1}$. At about 15K the dissociation process with another activation energy $E_{t,2}$ begins to dominate in DBE system. We eliminate the possibility of energy-transfer path that the lower-state (D^0,X) is converted into the higher-state (D^0,X) (i.e., $(D^0,X)_{n=1} \rightarrow (D^0,X)_{n=2}$ or $(D^0,X)_{n=2} \rightarrow (D^0,X)_{n=3}$) since $I^*_{(D^0,X)_{n=1,2,3}}$ decrease all together as the temperature is increased to 24 K.

The dissociation of the (D^0,X) system can obey four different general processes according to the dissociation of (A^0,X) system [28]. Thus we can compare the measured energies $E_{t,i}$ with the dissociation energy $E_{Ta,b,c,d}$ corresponding to each of these processes. The four general processes are written as:

(a) Dissociation resulting in a free exciton

$(D^0,X) \rightarrow D^0 + X$, $E_{Ta} = E(D^0,X) = E^b_{D^0,X}$.

(b) Dissociation resulting in one free electron and one free hole:

$$(D^0,X)\rightarrow D^0+e+h,\ E_{Tb}=E^b_{D^0,X}+E_X.$$

(c) Dissociation resulting in one free electron:

$$(D^0,X)\rightarrow(D^+,X)+e,\ E_{Tc}=E^b_{D^0,X}+E_X-E(D^0,h)=E_{Tb}-E(D^0,h)<E_{Tb}$$

(d) Dissociation resulting in two free electrons and one free hole:

$$(D^0,X)\rightarrow D^++e+e+h,\ E_{Td}=E_{Tb}+E_D>>E_{Tb}.$$

In CdTe, we know that $\Delta_{LT}=0.65meV$, $E_X=10.5meV$, $E_g=1.6069eV$ [37]. First, we consider the dissociation process (a) shown above. This process predicts an activation energy $E_{t1}=E^b_{D^0,X}$. It is obvious that the dissociation process (a) cannot cause the drop of $I^*_{(D^0,X)_{n=1,2,3}}$ associated with energy $E_{t,1}$ since $E_{t,1}$ is a very small value compared with $E_{Ta,b,c,d}$ (see columns 4 and 5 of Table IV), the process (c)-(d) can't either. That indicates that there exists another energy-transfer path. $E_{t,1}$ is very close to the longitudinal-transverse energy Δ_{LT} (=0.65meV). At the lowest temperature, most of the exciton-polaritons reside in the bottleneck region of the LPB. When the temperature is raised, the population of excitons coupled with photons in the LPB (to be abbreviated as X_{LPB}) is decreasing because some is converted into the longitudinal excitons (abbreviated as X_L). The population of excitons in LPB directly affect the population of exciton trapped to impurities. We explain $I^*_{(D^0,X)_{n=1,2,3}}$ decreasing with increasing temperature as the shortage of exciton source in the LPB due to the energy-transfer channel $X_{LPB}\rightarrow X_L$. Figure 5.3 displays the schematic diagram of this transfer channel associated with the activation energy

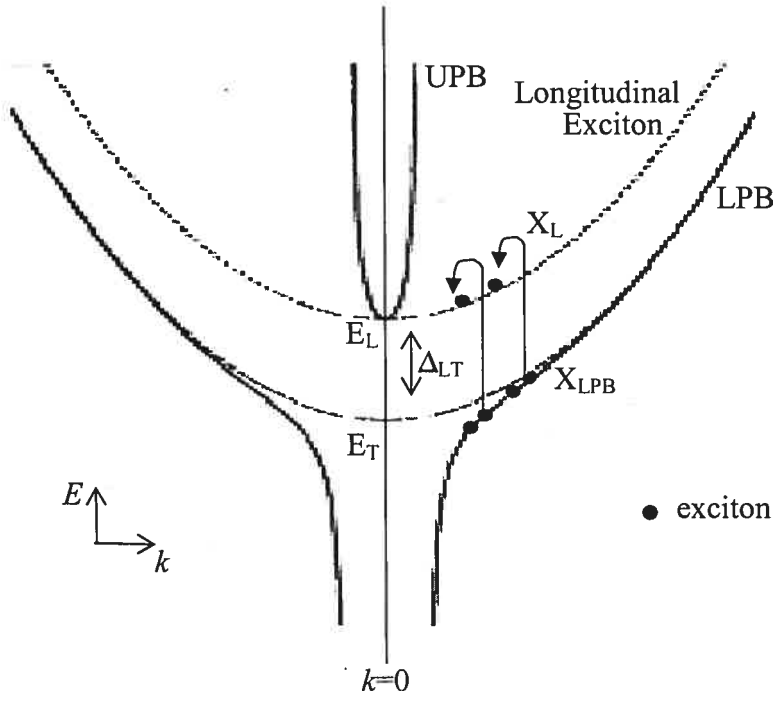

Figure 5.3 Schematic diagram of the dispersion cures of a 'bare' exciton (dashed curves) and an exciton-polariton (solid curves) in CdTe. The u-turn arrows indicate the transfer process of converting the excitons X_{LPB} in PLB into the longitudinal excitons X_L.

$E_{t,1}$ in CdTe.

The dissociation process (b) predicts the activation energy $E_{Tb} = E^{b}_{D^0,X} + E_X$ given in column 3 of Table IV. Comparison between column 3 and column 6 indicates that E_{Tb} and $E_{t,2}$ are very close. Thus we deduce that the dissociation procession (b) resulting in the liberation of a free electron and hole from a donor is another energy-transfer path associated with energy $E_{t,2}$.

In summary, as mentioned in the introduction, a simple formula based on the model of a two-step dissociation mechanism can be used to interpret the donor-bound-exciton transitions in high-purity InP studied by R. Benzaquen [14]. Here, we show that the behavior of the donor-bound-exciton transitions can also be described very well by the same formula in high-purity CdTe. At high-temperature region the dynamical properties of donor-bound exciton in high-purity CdTe agree with those in InP and the process (b) is responsible for donor-bound-exciton dissociation in CdTe. But not as expected, the dissociation path at low-temperature region is completely different. The energy-transfer path is $X_{LPB} \rightarrow X_L$ rather than the process (a) as in InP for the DBE dissociation at low temperature in CdTe. The dissociation path (a) does not happen when the temperature is increased from low to high region since figure 5.2 does not exhibit the slope corresponding to the third activation energy of about 3 meV.

CHAPTER 6

CONCLUSION

In this work, the dynamical properties of donor-bound excitons in a high-purity CdTe sample that is slightly doped with low donor to compensate for the acceptors, were studied using Fourier transform infrared and photoluminescence spectroscopic measurements.

We studied the optical characterization on a set of different CdTe samples. The FTIR PL spectrum of each sample shows one or several spectral features associated with (A^0, X), (D^0, X), (A^0, X)-LO, donor-acceptor pair and the native defect complexes. The CdTe LAH sample with very well (D^0, X) feature was the better one selected for our following study.

PL data were taken from 1.8 K to 24.0 K. PL spectra of high-purity CdTe display clearly the presence of emission peaks of donor-bound excitons at 1.5927 eV, 1.5933 eV, and 1.5938 eV, and furthermore, show asymmetric donor-bound-exciton transition peaks with the low-energy side broader than the high-energy side in low-energy region. In fact, while modeling the asymmetric transitions to gain an ideal fits, we have tried to use several asymmetric distribution functions including Gumbel, Genlogistic, Fisk, Weibull and Lsqdlrtz lineshapes. The asymmetric peaks failed to agree with these tested asymmetric functions. At last, the Fano lineshape

function was found to be the closest to our ideal model. Fano interference is a typical feature of the optical spectrum of low-dimensional semiconductors. We have introduced Fano interference in detail in the second chapter. The $(D^0, X)_{n=1}$ transition matches pure and simple Fano lineshape with negative q although it is not exactly real Fano interference, and $(D^0, X)_{n=2,3}$ have approximate Lorentzian lineshapes which describe the basic lineshapes for a homogenous broadening. According to the uncertainty principle and measurement of PL spectra, the values of the lifetime broadening are of the order of 0.1 meV, which approximately correspond to the radiative recombination lifetimes of the donor-bound exciton, around 6 ps.

In order to verify the spectral features of CdTe sample, we study the excitations with PLE measurements at energies of interest to our studies. Three strong spectral features which are associated with $(D^0, X)_{n=1,2,3}$ recombinations are observed in the PLE spectrum of acceptor-bound excitons. This might indicate that the short-lived lifetimes of $(D^0, X)_n$ result in exciton escape from the binding of donors. The most possible reason for the presence of $(D^0, X)_{n=1,2,3}$ peaks in the PLE spectrum of acceptor-bound excitons is that free and bound excitons are constantly converted each in the other.

We analyzed the temperature dependence of integrated intensities of the n =1, 2 and 3 components of the donor bound-exciton transitions in high-purity CdTe in detail by using a simple formula. This formula is based on the model of a two-step dissociation mechanism. We showed that, the behaviors of the

donor-bound-exciton transitions are welldescribed approximately by this formula. A remarkable feature of this model is that it includes two energy-transfer channels usually corresponding to two activation energies. When the temperature increases to about 15K, we got a very small activation energy which is lower than those of all the dissociation processes expected. And this energy is associated with the dispersion relation of exciton-polariton. At the lowest temperature, most of the exciton-polaritons occupy the positions of the bottleneck region of the lower-polariton-branch. Some of the excitons in the lower-polariton-branch state are converted into the longitudinal excitons with temperature increasing so that the population of excitons bound to donors becomes small. This energy-transfer channel from lower-polariton-branch excitons to longitudinal excitons results in the lower activation energy, i.e., the first drop of PL integrated intensity $I^{*}_{(D^0,X)_{n=1,2,3}}$ of CdTe sample. Exciton-polariton dispersion thus play a very important role in the optical properties of semiconductors at low temperature. When the temperature is further increased to 24.0 K, the second actvation energy with a bigger value appears within this temperature range. As expected, this activation energy agrees with the dissociation process controlled by the liberation of free electrons and holes from donors. Compared with the results in high-purity InP studied by Robert Benzaquen [14], the dissociation channel with the liberation of a free electron and a free hole from a shallow neutral donor does not happen as expected at the low-temperature region in CdTe. But at the high-temperature region the dynamical behavior of donor-bound excitons becomes very well identical.

To summarize, our results clearly demonstrated that shallow donor-bound excitons in high-purity CdTe have the dynamical behavior of two energy-transfer paths in the 1.8-24.0 K range by the measurements of temperature-dependent photoluminescence. One path is lower-polariton-branch excitons transfer to longitudinal excitons and another one is liberation of free electrons and holes from donors. Undoubtedly, it would be very meaningful in the future to study the dynamical properties of acceptor-bound excitons and other exciton complexes. Furthermore, it remains to understand why the emission lines of donor-bound excitons are so well described by a Fano profile since this cannot be explained by the interference between a discrete state and a continuum.

REFERENCES

[1] Razeghi M and Duchemin J P 1984 *J. Cryst. Growth* **70** 145

[2] NA LI, NING LI, W. LU, X. Q. LIU et al., *Superlattices and Microstructures, Vol. 26, No. 5,1999*

[3] Gallant M, Puetz N, Zemel A and Shepherd F R 1988 *Appl. Phys. Lett.* **52** 733 CdTe::: **1.** G.N. Panin, C.Diaz-Guerra and J.Piqueras, Semicond. Sci. Technol.13, 576, (1998).

[4] MH. Aslan, W. Song, J. Tang, D. Mao, and RT. Collins, D. H. Levi and R. K. Ahrenkiel, S. C. Lindstrom and M. B. Johnson, Mat. Res. Soc. Symp. Proc., 485 p.203 (1998).

[5] B. Monemar, E. Molva , and, Le Si Dang, *Phys. Rev. B* 33, 1134–1145 (1986)

[6] F. V. Wald, *Rev. Phys. Appl.* Vol. **12** #2 (1977), 277

[7] R. O. Bell, *Rev. Phys. Appl.* Vol. **12** #2 (1977), 391

[8] J. Aguilar-Hernandez, Gerardo Contreras-Puente at al., *Jpn. J. Appl. Phys.*, Vol. **33**, p37-41 1994

[9] K. Durose, P.R. Edwards, D.P. Halliday, J. Crystal Growth **197**, 733 (1999).

[10] M. Rami, E. Benamar, M. Fahoume, F. Chraibi, and A. Ennaoui, M.J. CONDENSED MATTER Vol. 3, Num. 1, 66 (2000)

[11] T. Takahashi and S. Watanabe, \Recent Progress in CdTe and CdZnTe Detector," IEEE Trans. Nucl. Sci., vol. 48, no. 4, pp.950-959, 2001.

[12] J A Godines, A Villegas, Yu Kudriavtsev, R Asomoza et al., Semicond. Sci. Technol. **19** (2004) 213–218

[13] R. Benzaquen and R. Leonelli, *Phys. Rev. B* : **59**, 1973–1985 (1999)

[14] R. Benzaquen and R. Leonelli, *Phys. Rev. B*, **52**, 1485–1488 (1995)

[15] Emil S. Koteles and J. Y. Chi, *Phys. Rev. B* **37**, 6332–6335 (1988)

[16] Satoru Seto and Akikazu Tanaka, *J. Appl. Phy.*, **64**(7), 3658-3662,1988

[17] S. Suga, W. Dreybrodt, F. Wilmann, P. Hiesinger, and K. Cho, *Solid State Commun.* **15**, 871 (1974)

[18] P. Hiesinger, S. Suga, F. Wilmann, and W. Dreybrodt, *Phys. Status Solidi B* **67**, 641 (1975)

[19] A. Nakamura and C. Weisbuch, *Solid-state Electron.* **21**, 1331 (1978)

[20] J. L. Pautrat, J. M. Francou, N. Magnea, E. Molva, and K. Saminadayar, J. *Cryst. Growth* **72**, 194(1985)

[21] C. F. Klingshirn, *Semiconductor Optics*, Chapter 11: Exciton, p.161, and, Chapter 15: *Optical Properties of bound and Localized Exciton and of defect States*, p.240

[22] J. R. Haynes, Phys. Rev. Lett., 4: 361(1960)

[23] Halstead, R. E. and Aven, M., Phys. Rev. Lett. **14**, 64 (1965).

[24] Roberto Benzaquen, Thèse : *Caractérisation optique et électrique d'Inp et de multipuits quantiques $Ga_{0.47}In_{0.53}As/InP$ obtenus par épitaxie à jets chimiques*, 1995

[25] Francou, J. M., Saminadayar, K., and Pautrat, J. L., Phys. Rev. B **41**, 12035 (1990).

[26] Molva, E., Pautrat, J. L., Saminadayar, K., Milchberg, G., and Magnea, N., Phys. Rev. B **30**, 3344 (1984).

[27] R. Benzaquen, M. Benzaquen, S. Charbonneau, P. J. Poole, T. Sudersena Rao, C. Lacelle, and A. P. Roth and R. Leonelli, *Phys. Rev.* B 50, 16964–16972 (1994)

[28] D. Bimberg and M. Sondergeld, and E. Grobe, *Phys. Rev. B*: **4**, 3451-3455 (1971)

[29] D.E. Cooper and P.R. Newman, Phys. Rev. B, 39, 7341-7440 (1989)

[30] Y. Toyozawa, On the dynamical behavior of an exciton. *Prog. Theor. Phys. Suppl.* **12**, 111-140 (1959)

B. Hõnerlage, U. Schtõder : *Phys. Rev. B*, **16**: 3608 (1997)

[31] C. Weisbuch and R. Ulbrich, in *Light Scattering in Solids* III, Vol. 57 of Topics in Applied Physics, edited by M. Cardona and G. Güntherodt (Springer, New York, 1982)

[32] E. L. Ivchenko, in *Excitons*, edited by E. I. Rashba and M. D. Sturge (North-Holland, Amsterdam, 1982), p. 141.

[33] Emil S. Koteles, *in Excitons*, edited by E. I. Rashba and M. D. Sturge (North-Holland, Amsterdam, 1982), p. 83.

[34] T. Steiner and M. L. W. Thewalt, E. S. Koteles and J. P. Salerno, Phys. Rev. B **34**, 1006 (1986)

[35] Peter Y. Yu and Manuel Cardona, in *Fundamental of Semiconductors* of Physics and Materials Properties, 3rd Edition (Springer, Berlin)

[36] Farid Askary and Peter Y. Yu, *Phys. Rev. B,* **31**, 6643 (1985)

[37] Semiconductors: *Data Handbook*, **Chapter 3** II-VI compounds, 3.19 Cadmium Telluride (CdTe)

[38] T Hayaishit, Y MoriokaS et al., *J. Phys.* B: At. Mol. Phys. **17** (1984) 3511-3527.

[39] V Bellaniy, L Vi˜nayz, R Heyx and K Ploog, *Semicond. Sci. Technol.* **11** (1996) 1411–1415.

[40] M. Dinu and D. D. Nolte, M. R. Melloch, *Phys. Rev.* B, Vol. 56, 4, 1987 (1997)

[41] V N Fleurovt and K A Kikoinj, *J. Phys.* C: Solid State Phys., 15 (1982) 3523-3537.

[42] S. Y. Savrasov and O. K. Andersen, *Phys. Rev. lett.*, Vol. 77, 4430 (1996)

[43] Fano U 1961, *Phys. Rev.* **124** 1866-78

[44] J. C. Phillips, Excitons, in *The Optical Properties of Solids*, ed. By J. Tauc (Academic, New York 1966), pp. 155-184

[45] S. Glutsch, Excitons in Low-Dimensitonal Semiconductors, Springer-Verlag Berlin Heidelberg New York 2004

[46] Edited: K. Cho, *Topics in Applied Physics*, Vol. 14, '*Exciton*', Chapter 3 Bound Exciton in Semiconductors

[47] Jaesun Lee and N. C. Giles, D. Rajavel and C. J. Summers, *Phys. Rev. B*: **49**, 1668–1676 (1994)

[48] C. F. Klingshirn, *Semiconductor Optics*, **Chapter 24**, Experimental techniques, p.402

APPENDIX I

The software MATLAB 6.1 was used to analyse the result. By the method of approximation of least squares we use Lsqdlrtz, Lorentzian or Fano lineshapes functions to fit the peaks. In fact, while modeling the transitions we met a great difficult to fit the asymmetric $(D^0, X)_1$ transition at the low energy region with the low-energy side broader than the high-energy side. To get ideal fitting curve, we have tested several asymmetric distribution functions such as Gumbel, Genlogistic, Fisk, Weibull and lsqdlrtz functions to fit asymmetric transition. Finally, the Fano lineshape function was found to be a nearly ideal model.

Parameters of CdTe sample, such as the amplitude *I*, the peak position λ^{-1} (cm^{-1}), the energy position E_0 *(eV),* the lineshape parameter q and the peak width σ (cm^{-1}), extracted from Fano fits of donor bound-exciton transitions $(D^0, X)_{n=1,2,3}$, for temperature between 1.8 *K* and 24.0 K, are shown in Table V.

Table V Parameters I, λ^{-1}, q, and, σ of CdTe sample extracted from Fano fits of donor bound-exciton transitions for temperature between 1.8 K and 24.0 K.

Temperaure (*K*)	Amplitude *I*		
	Peak a	Peak b	Peak c
1.8	0.9780	0.1965	0.1241
1.9	0.9784	0.1962	0.1225
2.0	0.9725	0.1963	0.1232
2.5	0.9713	0.2110	0.1193
3.3	0.9471	0.2663	0.1272
4.2	0.9417	0.3361	0.1493
4.5	0.9194	0.3343	0.1454
4.8	0.9296	0.3450	0.1491
5.1	0.9198	0.3708	0.1585
5.4	0.9191	0.3767	0.1572
6.6	0.9075	0.4513	0.1880
7.1	0.7627	0.4432	0.1875
7.5	0.7513	0.4232	0.1709
7.7	0.7530	0.4128	0.1679
8.3	0.7366	0.4449	0.1842
9.2	0.7300	0.4476	0.1792
9.5	0.7079	0.4367	0.1788
10.2	0.6815	0.4404	0.1730
10.9	0.7014	0.4871	0.1926
11.4	0.6959	0.4706	0.1741
11.8	0.6793	0.4712	0.1833
12.3	0.6674	0.4860	0.1795
13.0	0.6465	0.4699	0.1719
14.2	0.6217	0.4761	0.1823
15.1	0.6155	0.4711	0.1837
15.8	0.6034	0.4615	0.1827
16.0	0.5930	0.4628	0.1790

17.1	0.5501	0.4511	0.1879
18.0	0.5087	0.4715	0.1650
19.1	0.4507	0.3888	0.1345
22.2	0.5494	0.4471	0.1122
23.1	0.5142	0.4710	0.1322
24.0	0.5063	0.3943	0.1204
Temperature (*K*)	Position λ^{-1} (cm^{-1})		
	Peak a	Peak b	Peak c
1.8	0.1570	4.8033	8.8206
1.9	-0.1741	4.4723	8.4925
2.0	0.0834	4.6598	8.7181
2.5	-0.1756	4.4232	8.5296
3.3	0.1687	4.7408	8.8453
4.2	0.0703	4.6494	8.7478
4.5	0.1741	4.6739	8.8485
4.8	0.1672	4.6811	8.8542
5.1	0.1031	4.5763	8.7635
5.4	0.0940	4.5907	8.7579
6.6	0.0908	4.6050	8.7609
7.1	0.3058	4.6996	8.9298
7.5	0.0448	4.4832	8.7641
7.7	0.2170	4.6970	8.8955
8.3	0.1244	4.5406	8.8071
9.2	0.1957	4.6912	8.8603
9.5	0.3264	4.8048	9.0149
10.2	0.1825	4.6588	8.8940
10.9	0.1905	4.6237	8.8324
11.4	0.1128	4.6398	8.8255
11.8	0.2542	4.7099	8.9196
12.3	0.0959	4.5818	8.8064
13.0	0.1039	4.6267	8.7908

14.2	0.0004	4.5509	8.6474
15.1	0.1147	4.7194	8.7957
15.8	0.1346	4.7916	8.9359
16.0	0.2242	4.8591	8.9023
17.1	0.3812	4.9301	9.0931
18.0	0.4354	4.7300	9.1459
19.1	0.3895	4.9440	9.2994
22.2	0.3031	4.6870	8.8993
23.1	0.5134	4.7427	8.9856
24.0	0.2592	4.9302	9.0923
Temperature (K)	Lineshape parameter q		
	Peak a	Peak b	Peak c
1.8	-8.4980	-28.7568	-168.6305
1.9	-8.5945	-28.7476	-168.6304
2.0	-7.4430	-28.7415	-168.6337
2.5	-8.2717	-28.7359	-60.403
3.3	-8.1697	-25.7867	-169.4385
4.2	-8.9592	-28.7054	-60.4115
4.5	-6.2250	-28.6929	-60.4132
4.8	-6.5128	-28.6925	-60.4144
5.1	-6.1117	-28.6919	-60.4141
5.4	-6.5157	-28.7346	-60.3945
6.6	-6.3298	-28.6896	-60.4146
7.1	-4.8077	-28.6635	-60.4185
7.5	-5.4400	-28.6434	-60.4228
7.7	-5.8273	-28.6976	-60.4209
8.3	-5.2524	-28.6349	-60.4274
9.2	-5.8471	-28.6255	-60.4327
9.5	-5.8513	-28.6258	-60.4330
10.2	-5.8332	-28.6261	-60.4332
10.9	-5.3127	-28.6853	-60.4222

11.4	-6.4608	-28.6258	-60.4362
11.8	-5.9618	-28.6372	-60.4377
12.3	-5.8500	-28.6975	-60.4214
13.0	-6.6439	-28.6212	-60.4435
14.2	-7.1463	-28.6861	-60.4288
15.1	-7.5328	-28.6003	-60.4513
15.8	-7.8318	-28.5961	-60.4374
16.0	-7.5256	-28.5986	-60.4513
17.1	-5.4445	-28.4892	-60.4410
18.0	-3.4970	-28.6367	-60.4580
19.1	-4.4364	-28.4810	-60.4403
22.2	-4.1547	-28.4586	-60.4401
23.1	-3.1102	-28.4429	-60.4389
24.0	-4.9350	-28.4269	-60.4419

Temperature (K)	Peak width σ (cm^{-1})		
	Peak a	Peak b	Peak c
1.8	0.8906	1.2889	0.7910
1.9	0.8928	1.2947	0.8118
2.0	0.8404	1.3340	0.7171
2.5	0.9120	1.3560	0.8380
3.3	0.9139	1.3610	0.8615
4.2	0.9206	1.3366	0.8163
4.5	0.9970	1.5608	0.7916
4.8	1.0037	1.5351	0.7929
5.1	1.0067	1.5105	0.7744
5.4	1.0055	1.4987	0.7829
6.6	1.0683	1.5643	0.8062
7.1	1.1009	1.7958	0.8655
7.5	1.0823	1.7033	0.8756
7.7	1.0800	1.6577	0.8155
8.3	1.1183	1.6983	0.8733

9.2	1.1277	1.6533	0.8075
9.5	1.1640	1.7068	0.8758
10.2	1.1725	1.7092	0.8236
10.9	1.2138	1.7151	0.9335
11.4	1.1970	1.6484	0.8776
11.8	1.1961	1.6898	0.9678
12.3	1.2385	1.6836	1.068
13.0	1.2419	1.6029	1.0572
14.2	1.2983	1.5472	0.8709
15.1	1.3273	1.6018	0.8256
15.8	1.3490	1.5863	0.7348
16.0	1.3665	1.5574	0.7746
17.1	1.4131	1.8518	0.8003
18.0	1.3923	2.3107	1.0143
19.1	1.4665	2.0831	0.6224
22.2	1.4693	2.1308	0.7699
23.1	1.7345	2.3180	0.8526
24.0	2.0094	2.3311	0.6706

Table VI Energy position parameter E_0 (eV) ($E_0 = 8.0678\times 10^3\times (\lambda^{-1} + a\times 10^4)$ of CdTe sample.

Temperaure (K)	Displacement of peak positons $a\times 10^4 (cm^{-1})$ ($E_0 = 8.0678\times 10^3\times (\lambda^{-1} + a\times 10^4)$ (eV))
1.8	1.2850
1.9	1.2850
2.0	1.2850
2.5	1.2850
3.3	1.2850

4.2	1.2850
4.5	1.2850
4.8	1.2850
5.1	1.2850
5.4	1.2850
6.6	1.2850
7.1	1.2850
7.5	1.2850
7.7	1.2850
8.3	1.2850
9.2	1.2849
9.5	1.2849
10.2	1.2849
10.9	1.2849
11.4	1.2849
11.8	1.2849
12.3	1.2849
13.0	1.2849
14.2	1.2848
15.1	1.2848
15.8	1.2848
16.0	1.2847
17.1	1.2847
18.0	1.2846
19.1	1.2846
22.2	1.2843
23.1	1.2843
24.0	1.2843

APPENDIX II

The integrated PL intensities $I^*_{(D^0,X)_{n=1,2,3}}$ of DBE peak of CdTe sample, at the temperatures between 1.8 K and 24.0 K, are from a, b, and, c peaks of Figure 4.

Table VI The integrated PL intensities $I^*_{(D^0,X)_{n=1,2,3}}$ of CdTe sample at different temperature.

Temperature (*K*)	$I^*_{(D^0,X)_{n=1,2,3}}/10^3$ (*arb.units*)		
	Peak *a* (*n=1*)	Peak *b* (*n=2*)	Peak *c* (*n=3*)
1.8	71.664	20.335	7.5431
2.0	59.413	17.812	5.7828
2.5	31.948	10.383	3.0364
3.3	19.736	7.792	2.1623
4.2	8.326	3.800	0.9503
4.5	6.073	3.152	0.5868
4.8	6.023	3.139	0.6564
5.1	4.853	2.667	0.5463
5.4	4.541	2.523	0.7009
6.6	4.579	3.067	0.6564
7.1	4.646	3.807	0.7656
7.5	4.349	3.490	0.7245
7.7	4.383	3.358	0.6811
8.3	4.161	3.404	0.7209
9.2	4.044	3.348	0.6609
9.5	4.109	3.399	0.7160
10.2	3.779	3.296	0.6350
10.9	6.023	3.139	0.7009
11.4	3.440	3.187	0.7107

11.8	3.532	3.272	0.7446
12.3	4.349	3.490	0.7245
13.0	2.933	2.636	0.5704
14.2	2.856	2.580	0.5255
15.1	2.689	2.453	0.4631
15.8	2.556	2.279	0.4278
16.0	2.430	2.495	0.4594
17.1	2.197	2.716	0.4107
18.0	1.527	1.840	0.2040
19.1	1.022	1.212	0.1170
22.2	1.016	1.136	0.1214
23.1	0.763	0.801	0.0753
24.0	0.646	0.980	0.1333